Model adaptation for hyperbolic systems with relaxation

Hélène Mathis, Clément Cancès, Edwige Godlewski, Nicolas Seguin

MODEL ADAPTATION FOR HYPERBOLIC SYSTEMS WITH RELAXATION

H. MATHIS, C. CANCÈS, E. GODLEWSKI, N. SEGUIN

Abstract. In numerous applications, a hierarchy of models is available to describe the phenomenon under consideration. We focus in this work on general hyperbolic systems with stiff relaxation source terms together with the corresponding hyperbolic equilibrium systems. The goal is to determine the regions of the computational domain where the relaxation model (so-called *fine model*) can be replaced by the equilibrium model (so-called *coarse model*), in order to simplify the computation while keeping the global numerical accuracy. With this goal in mind, a numerical indicator which measures the difference between the solutions of both models is developed, using a numerical Chapman-Enskog expansion. The reliability of the adaptation procedure is assessed on various test cases coming from two-phase flow modeling.

Key-words. Hyperbolic system, finite volume methods, relaxation, model adaptation, Chapman-Enskog expansion, two-phase flows.
Mathematics Subject Classification. 35L45, 65M08, 65M55, 35C20, 76T10

1. Introduction

Interface coupling of existing numerical codes. The problem we address enters in the framework of modeling of complex flows arising in industry. The phenomena we consider imply that we have to handle different scales both in time and space. It leads to the use of a hierarchy of models which differ according to these scales. As an example, one may think about water circuits in pressurized water reactors (PWR). It is clear that a complex model of phase transition has to be used in the steam generator or in the condenser while simpler models are sufficient to describe the flow in most parts of the pipes. Besides, in the case of loss-of-coolant accident, only much more accurate models should be able to describe these highly heterogeneous flows.

A direct consequence of the use of different models and numerical codes in disjoint parts of the computational domain is the development of theoretical and numerical techniques of coupling. The coupling has to be non intrusive because of the complexity of the codes under study, leading to methods which only make use of boundary conditions. This has been the subject of a series of works where several methods of coupling have been proposed for hyperbolic systems of partial differential equations [28, 27, 5, 4, 8, 16, 7, 6, 25, 13]. In all these works, the interface of coupling which separates two different models is fixed. Since the models are different, there is not a consensual way of coupling, it depends on conservation and continuity principles which may be in contradiction (see for instance the examples in [7, 5]). As a consequence, the results vary according to the method of coupling and the more the flux is disturbed at the coupling interface, the greater is the sensibility to the coupling method. In order to avoid the dependence of the results on the interface coupling, it is natural to locate it where its impact is the most reduced.

Optimization of the position of the interface. We aim at providing new tools to optimize the location of the interfaces, following the preliminary work [43]. The context is the following: assume that the overall flow can be fully described by an accurate model, the so-called *fine model*, which involves small scales. We aim at detecting the regions of the computational domain where this fine model can be replaced by a reduced one, the so-called *coarse model*, without deteriorating the accuracy of the results. This model can be obtained by setting the small scales to zero in the fine model. The whole procedure relies on the computation of a (numerical) indicator, depending on time, that allows to perform the cutting of the computational domain into fine and coarse sub-domains. Such an indicator has to measure the difference between the solutions of the fine model and of the coarse model. Therefore, being given a threshold, it suffices to check whether the indicator is less than this threshold or not. In the first case, this means that replacing the fine model by the coarse model is possible, without introducing too much error. In the latter case, we continue to use the fine model.

Of course, the development of such an indicator depends on the models under investigation. As mentioned above, we aim at applying our method to compressible models of two-phase flows. Due to their complexity of the underlying PDE's, see for instance [34, 22], we are not able to derive robust and guaranteed criteria to position the interface(s).

Nonlinear systems of balance laws and hyperbolic relaxation. We focus in this paper on hyperbolic systems with relaxation. The fine model basically takes the form

$$\partial_t W + \sum_{\alpha=1}^{d} \partial_\alpha F_\alpha(W) = \frac{1}{\varepsilon} R(W), \tag{1}$$

with the initial condition $W(0,x) = W_0(x)$, which governs the evolution of the state vector $W(x,t) : \mathbb{R}^d \times \mathbb{R}^+ \to \Omega$. System (1) is the so-called *fine model*. Following the pioneer works on hyperbolic systems with stiff relaxation [42, 17, 50], we assume that there exists a linear operator $P_1 : \mathbb{R}^n \to \mathbb{R}^k$ of rank $k < n$ such that $P_1 R(W) = 0$ for all W. In other words, if we denote $u = P_1 W$, system (1) includes k independent conservation laws

$$\partial_t u + \sum_{\alpha=1}^{d} \partial_\alpha P_1 F_\alpha(W) = 0.$$

We also assume that the equilibrium $R(W) = 0$ can be parameterized in terms of u, that is to say there exists $M : \mathbb{R}^k \to \mathbb{R}^n$ such that for all u we have $R(M(u)) = 0$. This leads to the definition of the equilibrium system

$$\partial_t u + \sum_{\alpha=1}^{d} \partial_\alpha P_1 F_\alpha(M(u)) = 0. \tag{2}$$

This is the so-called *coarse model*. Additional assumptions ensure that the solutions of the fine model tend to solutions of the coarse model when $\varepsilon \to 0$, see for instance [42, 17, 50, 49], or in other words, that the leading order of the solutions of the fine model (1) is governed by the coarse model (2).

As mentioned above, we aim at defining an indicator which measures the difference between the solution W of the fine model (1) and the solution u of the coarse model (2). The main tool we use is based on the classical first-order *Chapman-Enskog expansion*

$$W = M(P_1 W) + \varepsilon W_1 \tag{3}$$

which provides a representation formula of the first order term W_1. As a result, for some norm to be precised, $\|\varepsilon W_1\|$ appears to be the right quantity for estimating the difference between the fine model and the coarse model. At the numerical level, the same method can be applied. On the basis of classical Finite Volume schemes for the fine model (1), we perform a numerical Chapman-Enskog expansion which provides the numerical counterpart of $\|\varepsilon W_1\|$. Note that, since the source term in (1) is approximated in an implicit way, the computation of the numerical indicator $\|\varepsilon W_1\|$ does not require to solve (1). Other indicators could be derived from error estimates provided for instance in [49] between general balance laws and their equilibrium counterpart and in [38] in a more academic case but also accounting for the error due to the interface coupling. Such ideas will be used in some forthcoming works.

Application to dynamical model adaptation. Let us now come back to our original problem of coupling two models through a thin interface. If we have such an indicator at our disposal, we may think that we are able to efficiently guess the position of the interface. In order to assess the relevance of our indicator, we insert it in a completely adaptive algorithm which automatically selects on-the-fly the "good" model to use. More precisely, being given a threshold $\theta > 0$, we compare in each cell and at each time step our local indicator with θ: if it is greater than θ, we conclude that the difference between the two models is large, then the fine model is locally used; otherwise, we conclude that the coarse model can be used. Thus, at each time step, the computational domain is divided in several parts where the fine or the coarse model is used and at each interface, the two models are coupled. It is clear that this method is much too complex to hope any CPU time saving in the present form but we believe that this approach is a good test to understand the relevance of the indicator we develop here.

Comparisons with related methods. Many numerical methods exist to address model adaptation. However, our motivations prevent us from applying standard multiscale techniques to our problem since we are in a situation where the numerical methods are given and cannot be modified.

In particular, asymptotic preserving schemes (let us only refer to the pioneer works [36, 40, 31] and the reviews [37, 30]) are designed to switch from a numerical scheme for the fine model (1) to a numerical scheme for the coarse model (2) in such a way that consistency, stability (thus convergence) and accuracy of these numerical schemes are achieved independently of ε. Other similar techniques belong to the class of heterogeneous multiscale methods and micro-macro decompositions. See for instance [1, 39, 41] and also [23, 10, 14, 29, 19, 11, 38] for related works on coupling models with different scales.

Outline of the paper. In Section 2 we present the hyperbolic model with relaxation we consider. Starting from the theory of Chen, Levermore and Liu [17], we depict the general framework of hyperbolic systems with stiff relaxation. Performing a Chapman-Enskog expansion, we show that the smooth solutions of the relaxation system solve the associated equilibrium model up to second order terms. Thus we obtain an explicit formula of the first order term of the expansion, which is the indicator we use thereafter to perform the adaptation algorithm. The remaining part of this section is dedicated to the numerical schemes for the fine model and for the coarse model.

In Section 3 is presented the algorithm of model adaptation. The first step is the construction of the indicator. It is obtained by performing the same Chapman-Enskog expansion as in the previous section, but on the numerical scheme. As the coarse model is the hyperbolic limit of the fine relaxation model, we assume

that the numerical scheme we use preserves this asymptotic property, at least for the algorithm we provide in this section (despite this condition is not necessarily fulfilled in the examples proposed in Section 4). This section ends with a thorough description of the algorithm for model adaptation.

The Section 4 is dedicated to numerical illustrations of model adaptation. We present three different applications, where we compare the numerical solutions obtained using the fine model, the coarse model and the model adaptation. The first example is a direct application of previous sections. The systems are conservative and the entropy is strictly convex and satisfies the assumptions of [17]. The compatibility of the numerical scheme (asymptotic preserving property) allows us to perform the adaptation algorithm presented in Section 3. For this example, the convergence of the dynamically adapted numerical solution towards the numerical solution of the fine model is observed as the threshold parameter θ for model selection tends to 0. The second example models a phase transition flow. The entropy of the model is not strictly convex which leads to a degeneracy of the indicator for pure phases. The last example concerns the modeling of a compressible two-phase flow described by the Baer-Nunziato model [9]. This test case does not enter the frame of the previous sections since the fine model is not strictly hyperbolic and non conservative. It also involves an nonlinear source term. The coarse model is the so-called homogeneous two-fluid model, which is composed by four conservation laws (the Euler equations endowed with a transport equation on the fraction of volume of one phase). Here, we choose to drop the compatibility between the two numerical schemes. Thus we provide a numerical scheme for the coarse model that is not derived from the fine one. This implies that the numerical indicator cannot be deduced from a Chapman-Enskog expansion on the fine scheme, we thus provide a classical discretization of the first order term obtained in the continuous Chapman-Enskog expansion.

Remark 1.1. *In view of the numerical experiments of the last section, the reader could be surprised that the two last models do not enter into the framework developed in the rest of the paper, i.e. in Sections 2 and 3. Actually, for the sake of conciseness, the models and methods are presented in the standard framework defined in reference works, as* [17]. *But our approach easily extends to the applications we have in mind, which come from nuclear thermohydraulics, which lead to quite complex systems (non conservative, non convex entropy...), so that they do not fulfill the assumptions we make in Section 2.*

2. Hyperbolic system with relaxation

2.1. **Algebraic structure of relaxation.** We consider the system of hyperbolic equations with relaxation terms

$$\partial_t W + \sum_{\alpha=1}^{d} \partial_\alpha F_\alpha(W) = \frac{1}{\varepsilon} R(W), \tag{4}$$

with the initial condition $W(0,x) = W_0(x)$. The state vector $W(x,t) : \mathbb{R}^d \times \mathbb{R}^+ \to \Omega$ belongs to the convex set $\Omega \subset \mathbb{R}^n$ of admissible states. The flux and the source term $F_\alpha,\ R : \mathbb{R}^n \to \mathbb{R}^n,\ \alpha = 1, \dots, d$ are supposed to be smooth. System (4) will be refereed in the sequel as the *fine model*.

We place ourselves inside the theoretical framework of Chen, Levermore and Liu [17]. There exists a linear operator $P_1 : \mathbb{R}^n \to \mathbb{R}^k$ of rank k, $1 \leq k < n$, such that

$$P_1 R(W) = 0,\ \forall W \in \Omega.$$

The operator P_1 defines k conserved quantities $u = P_1 W$ that satisfy

$$\partial_t u + \sum_{\alpha=1}^{d} \partial_\alpha P_1 F_\alpha(W) = 0.$$

There also exists another linear operator $P_2 : \mathbb{R}^n \to \mathbb{R}^{n-k}$ of rank $n-k$ such that the operator $\mathbb{P} = \begin{pmatrix} P_1 \\ P_2 \end{pmatrix}$ is nonsingular. Defining $\forall W \in \Omega$

$$f_1(P_1 W, P_2 W) = P_1 F(W), \quad f_2(P_1 W, P_2 W) = P_2 F(W),$$
$$r(P_1 W, P_2 W) = P_2 R F(W),$$

and setting $v = P_2 W$ we can rewrite the system (4) as

$$\partial_t u + \sum_{\alpha=1}^{d} \partial_\alpha f_{1,\alpha}(u, v) = 0, \tag{5}$$

$$\partial_t v + \sum_{\alpha=1}^{d} \partial_\alpha f_{2,\alpha}(u, v) = \frac{1}{\varepsilon} r(u, v). \tag{6}$$

The solutions of $R(W) = 0$ are called equilibrium Maxwellians. The manifold of Maxwellians $\mathcal{M} = \{W \in \Omega \mid R(W) = 0\}$ is parameterized in terms of the k conserved quantities $u = P_1 W$ and we can define a mapping $M \colon P_1\Omega \to \mathcal{M}$ such that u uniquely determines a local equilibrium value $W_{eq} = M(u) \in \mathcal{M}$ and $P_1 M(u) = u$ for all $u \in \mathbb{R}^k$. Let us also introduce the smooth map $v_{eq} : P_1\Omega \to P_2\Omega$ defined by $v_{eq}(u) = P_2 M(u)$. Then $r(u, v_{eq}(u)) = 0$, $\forall u \in P_1\Omega$. Furthermore we assume that the mapping

$$v \longmapsto r(u, v) \tag{7}$$

is invertible on a neighborhood of $v_{eq}(u)$.

When ε is small with respect to the characteristic variables of the system (4), the dynamics are asymptotically described by the so-called equilibrium system of conservation laws

$$\partial_t P_1 W + \sum_{\alpha=1}^{d} \partial_\alpha P_1 F_\alpha(M(P_1 W)) = 0,$$

that can also be written

$$\partial_t u + \sum_{\alpha=1}^{d} \partial_\alpha f_{1,\alpha}(u, v_{eq}(u)) = 0. \tag{8}$$

System (8) corresponds to what we call *coarse model*.

Assume now that the relaxation system (4) is endowed with a convex entropy $\Phi : \Omega \to \mathbb{R}$ satisfying:

(i) $\partial_{WW}\Phi(W)\partial_W F(W) \cdot \xi$ is symmetric $\forall W \in \Omega$ and $\xi \in \mathbb{R}^d$,
(ii) $\partial_W \Phi(W) R(W) \leq 0$, $\forall W \in \Omega$.

The condition (i) is the classical Lax condition for hyperbolic conservation laws. It ensures the existence of an entropy flux $\Psi : \Omega \to \mathbb{R}^d$ such that

$$\partial_W \Phi(W)\partial_W F(W) = \partial_W \Psi(W), \ \forall W \in \Omega. \tag{9}$$

Every classical solution of (4) satisfies

$$\partial_t \Phi(W) + \sum_{\alpha=1}^{d} \partial_\alpha \Psi_\alpha(W) = \frac{1}{\varepsilon} \partial_W \Phi(W) \cdot R(W), \tag{10}$$

and the second condition (ii) implies that the relaxation system is entropy dissipative since the right-hand side of (10) is non-positive. Besides the restriction of the entropy pair (Φ, Ψ) on the equilibrium manifold $\mathcal{M}$

$$\phi(u) := \Phi(M(u)), \quad \psi(u) := \Psi(M(u)),$$

gives an entropy pair (ϕ, ψ) for the system (8), so that the equilibrium system is hyperbolic (see [17] for a detailed proof).

2.2. **Chapman-Enskog expansion and dissipation.** We now focus on the relaxation system (5-6). Let us recall the classical result based on the Chapman-Enskog expansion.

Proposition 2.1. *Up to ε^2 terms, the smooth solutions of the relaxation system (5-6) formally satisfy*

$$\partial_t u + \sum_{\alpha=1}^{d} \partial_\alpha f_{1,\alpha}(u, v_{eq}(u)) = -\varepsilon \left(\sum_{\alpha=1}^{d} \partial_\alpha \nabla_v f_{1,\alpha}(u, v_{eq}(u)) \right) v_1, \tag{11}$$

$$v = v_{eq}(u) + \varepsilon v_1, \tag{12}$$

where

$$\begin{aligned} v_1 = \big(\nabla_v r(u, v_{eq}(u))\big)^{-1} \Bigg[& \sum_{\alpha=1}^{d} \partial_\alpha f_{2,\alpha}(u, v_{eq}(u)) \\ & - \nabla v_{eq}(u)^T \sum_{\alpha=1}^{d} \partial_\alpha f_{1,\alpha}(u, v_{eq}(u)) \Bigg]. \end{aligned} \tag{13}$$

Proof. Let us consider the Chapman-Enskog expansion

$$v^\varepsilon = v_{eq}(u) + \varepsilon v_1 + \mathcal{O}(\varepsilon^2).$$

Plugging it into (5-6) leads to

$$\partial_t u + \sum_{\alpha=1}^{d} \partial_\alpha f_{1,\alpha}(u, v_{eq}(u)) = -\varepsilon \left(\sum_{\alpha=1}^{d} \partial_\alpha \nabla_v f_{1,\alpha}(u, v_{eq}(u)) \right) v_1 + \mathcal{O}(\varepsilon^2),$$

$$\partial_t v_{eq}(u) + \sum_{\alpha=1}^{d} \partial_\alpha f_{2,\alpha}(u, v_{eq}(u)) = -\nabla_v r(u, v_{eq}(u)) v_1 + \mathcal{O}(\varepsilon).$$

The first system of equations is exactly (11) up to ε^2 terms. If we multiply it by $\nabla v_{eq}(u)^T$ and combine it with the second system of equation, we obtain the expression of the first order correction term v_1 (13). □

Note that the first order term v_1 is merely an explicit function of u.

The system (11-13) is a closed system of order 2 which can be seen as an intermediate model between the fine model (5-6) and the equilibrium model (8): formally, smooth solutions of (11-13) solve (5-6) up to ε^2 and, on the other hand, when ε tends to 0 one recovers the equilibrium model (8).

For stability reasons, one may expect that the second order term in (11-13) is dissipative. Note that this hypothesis is not verified without further assumptions, but following [12] and [17], the existence of a uniformly convex entropy satisfying (i) and (ii) implies that the second order correction term of (11-13) is dissipative (this is the so-called sub-characteristic condition).

Remark 2.1. *Let us recall that the Chapman-Enskog expansion fails to be true near discontinuities, the above calculus being valid only for smooth solutions.*

2.3. **Numerical scheme.** We now detail the scheme associated with the fine model (5-6).

Let us consider a mesh $\mathcal{T}_h$ of the computational domain $\mathcal{D} \subset \mathbb{R}^d$ made of cells K, that are polygonal disjoint open subsets. If K and L are two neighboring cells (in the sequel we will use the notation $L \in \mathcal{N}(K)$) their common face is denoted $e_{KL} = \overline{K} \cap \overline{L}$ and n_{KL} is the outgoing unit normal to K. The notations $|K|$ and $|e_{KL}|$ refer to the volume of the cell K and the surface of the edge e_{KL} respectively. We denote Δt the time step and the sequence of time steps $(t^n)_n$ such that $t^{n+1} = t^n + \Delta t$, $\forall n \in \mathbb{N}$. We define the approximation of the initial data by

$$W_K^0 = \int_K W_0(x)dx.$$

The finite volume formulation is obtained integrating the system (5-6) on the space-time domain $[t^n, t^{n+1}] \times K$ and we introduce the two numerical fluxes F_1 and F_2, respectively consistent with the fluxes f_1 and f_2 in (5-6). The relaxation system is approximated using a splitting strategy between the convective part and the source term. Suppose the approximation W_K^n, $\forall K \in \mathcal{T}_h$, is known at time t^n and let us introduce the notation $Z_K^n = (u_k^n, v_K^n)^T = \mathbb{P}W_K^n$. For simplicity, the numerical schemes is expressed in terms of Z_K^n instead of W_K^n. In a first step, from t^n to an intermediate time $t^{n+1,-}$, the convective part is approximated by

$$u_K^{n+1,-} = u_K^n - \frac{\Delta t}{|K|} \sum_{L \in \mathcal{N}(K)} |e_{KL}| F_1(Z_K^n, Z_L^n, n_{KL}), \tag{14}$$

$$v_K^{n+1,-} = v_K^n - \frac{\Delta t}{|K|} \sum_{L \in \mathcal{N}(K)} |e_{KL}| F_2(Z_K^n, Z_L^n, n_{KL}). \tag{15}$$

Then the value $Z_K^{n+1,-}$ is taken as the initial data for solving the source term:

$$u_K^{n+1} = u_K^{n+1,-}, \tag{16}$$

$$v_K^{n+1} = v_K^{n+1,-} + \frac{\Delta t}{\varepsilon} r(u_K^{n+1}, v_K^{n+1}). \tag{17}$$

The classical implicit Euler scheme is chosen in order to ensure the unconditional stability of the second step. The key-point here is to assume that all the difficulty of this method is due to this implicit part, so that the underlying resolution may be costly and complex. For instance, alternative methods can be found in [24], and in [21] for high order time discretizations.

One may easily deduce a numerical scheme for the coarse model (8). Let us denote $Z_{eq,K}^n = \mathbb{P}M(u_K^n) = (u_K^n, v_{eq}(u_K^n))$. The first step remains unchanged with $Z_K^n = Z_{eq,K}^n$ plugged into (14). The second step reduces to take v at equilibrium. The resulting numerical scheme is simply

$$u_K^{n+1} = u_K^n - \frac{\Delta t}{|K|} \sum_{L \in \mathcal{N}(K)} |e_{KL}| F_1(Z_{eq,K}^n, Z_{eq,L}^n, n_{KL}), \tag{18}$$

$$v_K^{n+1} = v_{eq}(u_K^{n+1}). \tag{19}$$

The use of this numerical scheme avoids any computation of v: (15) is not used and the stiff source term has not to be solved (17).

In practice, the numerical scheme for the coarse model (8) can be different (see Section 4). Nonetheless, requiring the above compatibility between the two numerical schemes enables us to define the adaptation algorithm in a simpler way.

3. Model adaptation

As mentioned previously the problematic we are interested in is to guess where the fine model can be replaced by the coarse model.

The cutting of the computational domain into a fine and a coarse sub-domain relies on the use of an indicator. The computation of this indicator is described in this section. It corresponds to a discretization of the first order correction term v_1 resulting from the Chapman-Enskog expansion (see Section 2.2, proposition 2.1). This indicator allows us to realize the dynamical cutting of the space and time computational domain.

At the end of this section, we precise the adaptation algorithm based on the coupling of the relaxation model and of the equilibrium one at each sub-domain interfaces.

3.1. General ideas.

At each time step, the strategy is to detect the sub-domain (non necessarily connected) where the fine model can be replaced by the coarse one. Let $\mathcal{D}_f(t)$ (resp. $\mathcal{D}_c(t)$) be the sub-domain where the fine model (resp. the coarse model) has to be solved. We impose that the sub-partitions do not intersect:

$$\overline{\mathcal{D}_f(t)} \cup \overline{\mathcal{D}_c(t)} = \mathcal{D}, \quad \mathcal{D}_f(t) \cap \mathcal{D}_c(t) = \emptyset.$$

At the interfaces between the sub-domains $\overline{\mathcal{D}_f(t)} \cap \overline{\mathcal{D}_c(t)}$ a coupling strategy has to be applied.

The computation of the indicator is based on the Chapman-Enskog expansion described in Proposition 2.1. We make the assumption that the difference between the solution of the fine model (5-6) and the solution of the coarse model (8) can be measured by some norm of εv_1, defined by (12-13). Therefore, if $\|\varepsilon v_1\|$ is less than a given threshold, then the coarse model is solved and if $\|\varepsilon v_1\|$ is larger, the fine model is solved.

It is well-known that the Chapman-Enskog expansion is only valid for smooth solutions and in the neighborhood of the equilibrium manifold $\mathcal{M}$. here, we suppose that when the solution becomes discontinuous or far from $\mathcal{M}$, the indicator $\|\varepsilon v_1\|$ blows up. In these two cases, the model to solve is clearly the fine model.

A tolerance θ being given, the partitioning procedure reads as follow:

- The region where $\|\varepsilon v_1\| \leq \theta$ is chosen to be $\mathcal{D}_c(t)$. In that domain the error between the equilibrium model and the relaxed one is assumed to be negligible, so that the coarse model (8) is applied.
- The domain $\mathcal{D}_f(t)$ corresponds to the region where $\|\varepsilon v_1\| > \theta$ and the relaxation model (5-6) is solved inside.
- At the interfaces separating the sub-domains $\mathcal{D}_c(t)$ and $\mathcal{D}_f(t)$, a numerical coupling method, like the ones developed in [7, 15], is used.

Remind that the indicator εv_1 only depends on u (see (13)). Thus it is known on the whole domain, because u is solved in the fine and the coarse model.

3.2. Numerical indicator.

Let us now build the numerical indicator. To do so, we use the Chapman-Enskog expansion at the discrete level on the numerical scheme (14-17).

Proposition 3.1. *Let us consider the numerical scheme (14-17). Then, up to ε^2 terms, one has*

$$v_K^{n+1} = v_{eq}(u_K^{n+1}) + \varepsilon v_{1,K}^{n+1}, \tag{20}$$

where

$$v_{1,K}^{n+1} = \left(\nabla_v r(u_K^{n+1}, v_{eq}(u_K^{n+1}))\right)^{-1} \frac{1}{|K|} \sum_{L\in\mathcal{N}(K)} |e_{KL}| \left\{F_2(Z_{eq,K}^n, Z_{eq,L}^n, n_{KL}) + \nabla v_{eq}(\overline{u})^T F_1(Z_{eq,K}^n, Z_{eq,L}^n, n_{KL})\right\}, \tag{21}$$

with $Z_{eq,K}^n = \mathbb{P}M(u_K^n) = (u_K^n, v_{eq}(u_K^n))^T$ *and* $\overline{u}$ *satisfying*

$$\nabla v_{eq}(\overline{u})^T (u^{n+1} - u^n) = v_{eq}(u^{n+1}) - v_{eq}(u^n).$$

The term $v_{1,K}^{n+1}$ *is a first order approximation of* v_1 *at time* t^{n+1} *in cell* K*.*

Proof. We plug the ansatz (20) in the numerical scheme (14-17) and, noting $Z_{1,K}^n = (0_{\mathbb{R}^k}, v_{1,K}^n)^T$ for all $K \in \mathcal{T}_h$, we obtain

$$\begin{aligned} u_K^{n+1} = u_K^n + \frac{\Delta t}{|K|} \sum_{L\in\mathcal{N}(K)} |e_{KL}| \Big[& F_1(Z_{eq,K}^n, Z_{eq,L}^n, n_{KL}) \\ & + \varepsilon \big(\nabla_1 F_1(Z_{eq,K}^n, Z_{eq,L}^n, n_{KL})\big)^T Z_{1,K}^n \\ & + \varepsilon \big(\nabla_2 F_1(Z_{eq,K}^n, Z_{eq,L}^n, n_{KL})\big)^T Z_{1,L}^n \Big] + \mathcal{O}(\varepsilon^2), \end{aligned} \tag{22}$$

where $\nabla_\beta F_1(Z_1, Z_2, n)$, $\beta = 1, 2$, is the partial derivative of F_1 with respect to Z_β. We also obtain

$$\begin{aligned} v_{eq}(u_K^{n+1}) = v_{eq}(u_K^n) + \frac{\Delta t}{|K|} \sum_{L\in\mathcal{N}(K)} |e_{KL}| F_2(Z_{eq,K}^n, Z_{eq,L}^n, n_{KL}) \\ + \Delta t \big(\nabla_v r(u_K^{n+1}, v_{eq}(u_K^{n+1}))\big)^T v_{1,K}^{n+1} + \mathcal{O}(\varepsilon). \end{aligned} \tag{23}$$

Since v_{eq} is smooth, there exists $\overline{u}(.,.)$ such that:

$$\left[\nabla v_{eq}\left(\overline{u}(u^n, u^{n+1})\right)\right]^T (u^{n+1} - u^n) = v_{eq}(u^{n+1}) - v_{eq}(u^n).$$

Multiplying (22) by $\left[\nabla v_{eq}(\overline{u}(u_K^n, u_K^{n+1}))\right]^T$ and dropping terms of order ε leads to

$$v_{eq}(u_K^{n+1}) = v_{eq}(u_K^n) - \frac{\Delta t}{|K|} \nabla v_{eq}(\overline{u})^T \sum_{L\in\mathcal{N}(K)} |e_{KL}| F_1(Z_{eq,K}^n, Z_{eq,L}^n, n_{KL}).$$

Combining with (23) and dropping terms of order ε provides (21). Using the consistency of the numerical fluxes, it is easy to check that (21) is a consistent approximation of the continuous formula (13). □

Note that replacing the terms $v_{1,K}^n$ and $v_{1,L}^n$ into (22) using the expression (21) could allow us to determine the discrete counterpart of the parabolic system (11). Moreover, one can check that, as at the continuous level, the zeroth order part of (22) exactly is the coarse scheme (18-19).

In practice, the terms $\nabla v_{eq}(\overline{u}(u_K^n, u_K^{n+1}))$ and $(\nabla_v r(u_K^{n+1}, v_{eq}(u_K^{n+1})))^{-1}$ are respectively approximated by $\nabla v_{eq}(u_K^n)$ and $(\nabla_v r(u_K^n, v_{eq}(u_K^n)))^{-1}$ to make the computation of the indicator fully explicit.

We deduce the following indicator:

$$\begin{aligned} \mathcal{E}_K^{n+1} := & \varepsilon \left(\nabla_v r(u_K^n, v_{eq}(u_K^n))\right)^{-1} \frac{1}{|K|} \sum_{L\in\mathcal{N}(K)} |e_{KL}| \\ & \left[F_2(Z_{eq,K}^n, Z_{eq,L}^n, n_{KL}) + \nabla v_{eq}(u_K^n)^T F_1(Z_{eq,K}^n, Z_{eq,L}^n, n_{KL})\right]. \end{aligned} \tag{24}$$

This provides an indicator of the difference of the solutions given by the two schemes at time t^{n+1}, as an explicit function of the discrete solution (u_K^n), $\forall K \in \mathcal{T}_h$, (at time t^n) that is known within the whole computational domain.

3.3. **Adapted model and coupling.** In order to simplify the algorithm, the model adaptation is performed at each time step t^n. Assume that the subdivision of the computational domain into $\mathcal{D}_f(t^n) \times (t^n, t^{n+1})$ and $\mathcal{D}_c(t^n) \times (t^n, t^{n+1})$ is known. The adapted model is the following coupling problem $\forall n \in \mathbb{N}$:

$$\begin{cases} (4) \text{ solved in } \mathcal{D}_f(t^n) \times (t^n, t^{n+1}), \\ (8) \text{ solved in } \mathcal{D}_c(t^n) \times (t^n, t^{n+1}), \\ \text{coupling conditions in } \overline{\mathcal{D}_f(t^n)} \cap \overline{\mathcal{D}_c(t^n)} \times (t^n, t^{n+1}). \end{cases}$$

Several coupling conditions can be considered. In the following we favor state coupling [15, 7]. Let K be a cell belonging to the fine domain $\mathcal{D}_f(t^n)$ and L its neighbor belonging to the coarse domain $\mathcal{D}_c(t^n)$. Then at the edge e_{KL}, we impose $(u_L^n, v_{eq}(u_L^n))$ as Dirichlet boundary condition for the fine model and u_K^n as Dirichlet boundary condition for the coarse model: if $K \in \mathcal{D}_f(t^n)$ and $L \in \mathcal{D}_c(t^n)$, the numerical fluxes are

($\mathcal{C}1$) $\big(F_1(Z_K^n, Z_{eq,L}^n, n_{KL}), F_2(Z_K^n, Z_{eq,L}^n, n_{KL})\big)$ for the computation of $Z_K^{n+1,-}$ by the fine scheme (14-15),

($\mathcal{C}2$) $F_1(Z_{eq,L}^n, Z_{eq,K}^n, n_{LK})$ for the computation of Z_L^{n+1} by the coarse scheme (18), written on cell L.

This amounts to impose the continuity of u and $v = v_{eq}(u)$ through the coupling interface.

Remark 3.1. *One may impose other coupling constraints. For instance the equation on u being solved everywhere, one may impose the continuity of the flux f_1 through the interface e_{KL}. This strategy of flux coupling is not tested here but may have special interest in some cases (see for instance Section 4). However at the interface the fine and the coarse models are mostly equivalent, the fine model being close to equilibrium, thus all the coupling strategies may be supposed to provide similar results.*

3.4. **Adaptation algorithm.** We now detail the general algorithm of the dynamical coupling between the fine and the coarse models. Let W_K^n be the solution in the cell K known at time t^n to be updated to time t^{n+1}. The algorithm reads as follows:

A) For all cell $K \in \mathcal{T}_h$, compute the numerical error $\mathcal{E}_K^{n+1}$ given by (24)

B) For all cell $K \in \mathcal{T}_h$, if $[|\mathcal{E}_K^{n+1}| > \theta]$ then
   - $K \in \mathcal{D}_f(t^n)$

   Else
   - $K \in \mathcal{D}_c(t^n)$

C) At this stage, $\overline{\mathcal{D}_f(t^n)} \cup \overline{\mathcal{D}_c(t^n)} = \mathcal{D}$.
   For all cell $K \in \mathcal{T}_h$:
   - If $[K \in \mathcal{D}_f(t^n)$ and $\forall L \in \mathcal{N}(K), L \in \mathcal{D}_f(t^n)]$
     - Compute W_K^{n+1} using the numerical scheme (14-17).
   - If $[K \in \mathcal{D}_c(t^n)$ and $\forall L \in \mathcal{N}(K), L \in \mathcal{D}_c(t^n)]$
     - Compute W_K^{n+1} using the numerical scheme (18-19).
   - Else
     - Compute W_K^{n+1} using the state coupling method ($\mathcal{C}1$-$\mathcal{C}2$).

4. Numerical applications

We provide in this section some numerical examples to illustrate the reliability of the indicator (24), by applying it to the algorithm for model adaptation. We make a point of giving different models which present various pathologies. Indeed, we could have chosen to restrict ourselves to models which strictly fulfill the assumptions we

made. However, we prefer to address more complex systems which do not fully enter into the framework described in the previous sections, by applying the same ideas to problems which are more closely related to the applications we have in mind, which come from thermohydraulics in the context of nuclear reactors.

First we consider the academic case of the Chaplygin gas model, that consists in the barotropic Euler equations with relaxation. The simple form of the source term allows us to exhibit a dissipative convex entropy.

Then we consider a phase transition model. In that case the entropy is no longer strictly convex and the Chapman-Enskog expansion may not be valid. In particular, the indicator (24) vanishes in pure phases.

Finally we address the approximation of the solutions of the compressible seven-equation two-phase flow model. Although this model does not enter the frame of the section 2 (non convex entropy, non-strictly hyperbolic and non conservative model, incompatible numerical schemes for the fine and coarse models...), the adaptation process is carried out, providing a slightly different adaptation algorithm.

4.1. **Chaplygin gas model.** We first consider the academic model of the Chaplygin gas [47]. The one-dimensional problem we address corresponds to a fluid flow governed by the relaxation system

$$\begin{aligned} \partial_t \tau - \partial_x u &= 0, \\ \partial_t u + \partial_x \Pi &= 0, \\ \partial_t \mathcal{T} &= \frac{1}{\varepsilon}(\tau - \mathcal{T}). \end{aligned} \tag{25}$$

This model is also derived from the works of Suliciu [48]. The state variable τ and u stand for the specific volume and the velocity while $\mathcal{T}$ is a perturbed specific volume. The extended pressure law Π is defined by

$$\Pi(\tau, \mathcal{T}) = p(\mathcal{T}) + a^2(\mathcal{T} - \tau),$$

where p follows a perfect gas law $p = p(\tau) = \tau^{-\gamma}$, $\gamma > 1$.

The associated equilibrium system is obtained setting $\mathcal{T} = \tau$ and corresponds to the barotropic Euler equations in Lagrangian coordinates:

$$\begin{aligned} \partial_t \tau - \partial_x u &= 0, \\ \partial_t u + \partial_x p &= 0. \end{aligned} \tag{26}$$

A convex entropy of the Suliciu system is (see [18]):

$$\Phi(\tau, u, \mathcal{T}) = \frac{1}{2}|u|^2 + \frac{1}{1-\gamma}\mathcal{T}^{1-\gamma} + \frac{a^2}{2}(\mathcal{T}^2 - \tau^2) + (\mathcal{T}^{-\gamma} + a^2\mathcal{T})(\tau - \mathcal{T}).$$

The entropy is strictly convex and dissipative with respect to the source term under the so-called Whitham's condition

$$a^2 > \max_s(-p'(s)).$$

This condition also implies that the Chapman-Enskog expansion is dissipative, see for instance [12]. We consider Rusanov numerical fluxes [44] and, using the previous computations, we obtain the following numerical indicator

$$\begin{aligned} \mathcal{E}_K^{n+1} := \varepsilon T_{1,K}^{n+1} = &- \varepsilon \frac{1}{2\Delta x}(p(\tau_{K+1}^n) + p(\tau_K^n) - a_{K+1/2}(u_{K+1}^n - u_K^n) \\ &- p(\tau_K^n) - p(\tau_{K-1}^n) + a_{K-1/2}(u_K^n - u_{K-1}^n)). \end{aligned}$$

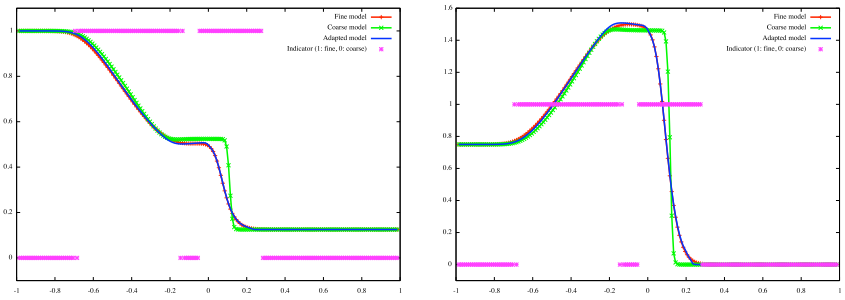

FIGURE 1. Density $1/\tau$ (top) and velocity (bottom) with 200 cells at time $T = 0.5$. The indicator corresponds to the characteristic function of $\mathcal{D}_f(T)$.

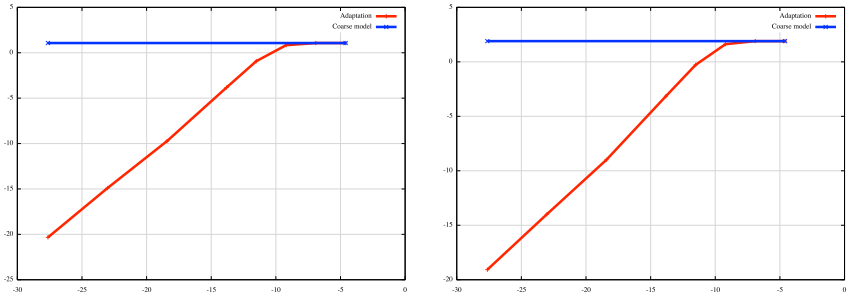

FIGURE 2. Error between model (R) and the model adaptation, w.r.t. θ: specific volume τ (left) and velocity (right)

Test case. Figure 1 presents the density and the velocity profiles for $\gamma = 1.4$ and $a = 1.5$. The initial data are $\tau_L = 1$, $u_L = 0.75$, $\tau_R = 8$, $u_R = 0$ and the discontinuity is applied at $x = 0$. The relaxation parameter is $\varepsilon = 10^{-6}$. The mesh contains 200 cells and threshold for the adaptation is $\theta = 10^{-6}$. One may check that our method of adaptation only uses the fine model in the regions of large variations of the solution. The results are very close to those with the fine model. One may also note that the results of the coarse model are quite different with: less diffusion and a different intermediate state.

In order to measure the sensitivity of the numerical results, the same test case is performed with different values of θ. In Figure 2, the L^1 norm of the difference between the adaptation algorithm and the fine model is plotted (red curves). The behavior is very satisfying: the error due to the adaptation tends to 0 as θ tends to 0. Of course, the error of the adaptation algorithm is bounded by the error of the coarse model (blue curves), which confirms that the adaptation method does not introduce additional numerical error, which could be caused by the interface couplings.

4.2. **Phase transition model.** We now address the numerical approximation of a liquid-vapor compressible flow. Each phase, denoted $\beta = 1$ or 2, is described by its own Equation of State (EoS) and thermodynamical quantities: ρ_β denotes the density, $\tau_\beta = 1/\rho_\beta$ the specific volume, e_β the internal energy. We assume that both phases are described by a perfect gas law, such that the pressure p_β, the

temperature T_β and the entropy of each phase are classically given by:

$$\begin{aligned} p_\beta(\rho_\beta, e_\beta) &= (\gamma_\beta - 1)\rho_\beta e_\beta, \\ T_\beta &= e_\beta, \\ s_\beta &= \ln\left(e_\beta \rho_\beta^{\gamma_\beta - 1}\right), \end{aligned}$$

where $\gamma_\beta > 1$ stands for the polytropic exponent. We also introduce the chemical potential $g_\beta = \dfrac{p_\beta}{\rho_\beta} - T_\beta s_\beta + e_\beta$.

The density of the fluid is related to those of both phases by the following relations

$$\begin{aligned} \rho &= \alpha\rho_1 + (1-\alpha)\rho_2, \\ (\rho^{-1} =) \quad \tau &= \varphi\tau_1 + (1-\varphi)\tau_2, \end{aligned}$$

where α and φ denote respectively the volume fraction and the mass fraction of the gaseous phase. The thermodynamical equilibrium of both phases corresponds to the equality of pressures, temperatures and chemical potentials. It is characterized by the following fractions at equilibrium:

$$\varphi_e(\rho) = \frac{\tau - \tau_2^*}{\tau_1^* - \tau_2^*}, \quad \alpha_e(\rho) = \frac{\rho - \rho_2^*}{\rho_1^* - \rho_2^*}, \quad \tau_1^* = \frac{1}{\rho_1^*}, \quad \tau_2^* = \frac{1}{\rho_2^*},$$

together with

$$\rho_1^* = \exp(-1)\left(\frac{\gamma_2 - 1}{\gamma_1 - 1}\right)^{\frac{\gamma_2}{\gamma_2 - \gamma_1}}, \quad \rho_2^* = \exp(-1)\left(\frac{\gamma_2 - 1}{\gamma_1 - 1}\right)^{\frac{\gamma_1}{\gamma_2 - \gamma_1}}.$$

These two constant densities define the saturation states. The fine model we consider corresponds to the Euler's equations coupled with a transport equation of the mass fraction (here in one dimension):

$$\begin{aligned} \partial_t \rho + \partial_x(\rho u) &= 0, \\ \partial_t(\rho u) + \partial_x(\rho u^2 + p) &= 0, \\ \partial_t(\rho E) + \partial_x((\rho E + p)u) &= 0, \\ \partial_t(\rho\varphi) + \partial_x(\rho u \varphi) &= \frac{1}{\varepsilon}(\varphi_{eq}(\rho) - \varphi), \end{aligned} \tag{27}$$

where $E = e + u^2/2$ stands for the total energy of the fluid and the complete equilibrium mass fraction is defined by

$$\varphi_{eq}(\rho) = \begin{cases} 1 & \text{if } \rho \le \rho_1^*, \\ \varphi_e(\rho) & \text{if } \rho_1^* \le \rho \le \rho_2^*, \\ 0 & \text{if } \rho_2^* \le \rho. \end{cases}$$

To close the system, we consider the EoS

$$p = p(\rho, e, \varphi) = (\gamma(\varphi) - 1)\rho e,$$

where $\gamma(\varphi) = \gamma_1\varphi + \gamma_2(1-\varphi)$.

Remark 4.1. *The entropy of the system is not strictly convex, as shown in* [35, 33, 2, 32]. *In particular, the source term in* (27) *vanishes when* $\rho \notin [\rho_1^*, \rho_2^*]$. *As a consequence, the map* (7) *is not invertible and the Chapman-Enskog expansion does not provide a dissipative system in the whole domain.*

Let us now present the equilibrium model. If $\alpha = 0$ (resp. $\alpha = 1$) then $\varphi = 0$ (resp. $\varphi = 1$) and we directly recover the Euler equations for the pure phase. If

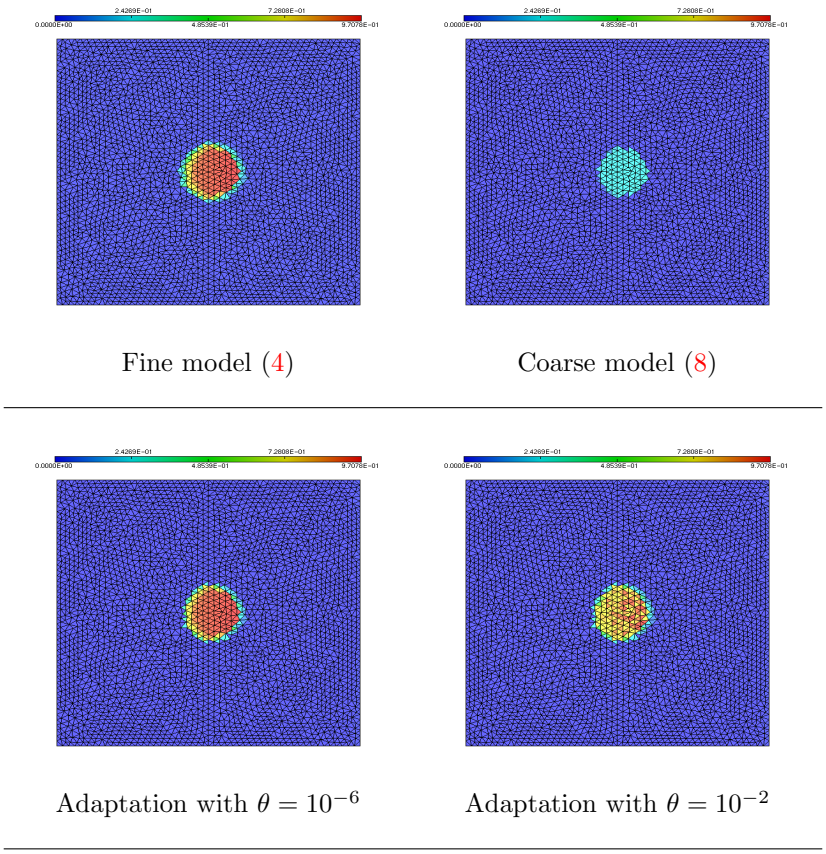

Fine model (4) | Coarse model (8)

Adaptation with $\theta = 10^{-6}$ | Adaptation with $\theta = 10^{-2}$

FIGURE 3. Solution after the first interaction: mass fraction φ

$0 < \alpha < 1$, the limit $\varepsilon \to 0$ leads to $g_1 = g_2$: the thermodynamical equilibrium is reached. This asymptotic defines the coarse model:

$$\begin{aligned} \partial_t \rho + \partial_x(\rho u) &= 0, \\ \partial_t(\rho u) + \partial_x(\rho u^2 + p) &= 0, \\ \partial_t(\rho E) + \partial_x((\rho E + p)u) &= 0, \end{aligned} \tag{28}$$

where $p = p(\rho, e, \varphi_{eq}(\rho))$ that is

$$p = p(\rho, e) = \begin{cases} (\gamma_1 - 1)\rho e & \text{if } \rho \leq \rho_1^*, \\ (\gamma_1 - 1)\rho_1^* e & \text{if } \rho_1^* \leq \rho \leq \rho_2^*, \\ (\gamma_2 - 1)\rho e & \text{if } \rho_2^* \leq \rho. \end{cases} \tag{29}$$

To carry out the adaptation, we have to compute the indicator, which is easily deduced from identity (13) and reads

$$\varphi_1 = (\rho\varphi_{eq})'(\rho)\partial_x(\rho u) - \partial_x(\rho u \varphi_{eq}(\rho)).$$

The numerical schemes we use are based on the Rusanov scheme [44]. The discrete indicator arises from formula (24), in which the numerical fluxes F_1 and

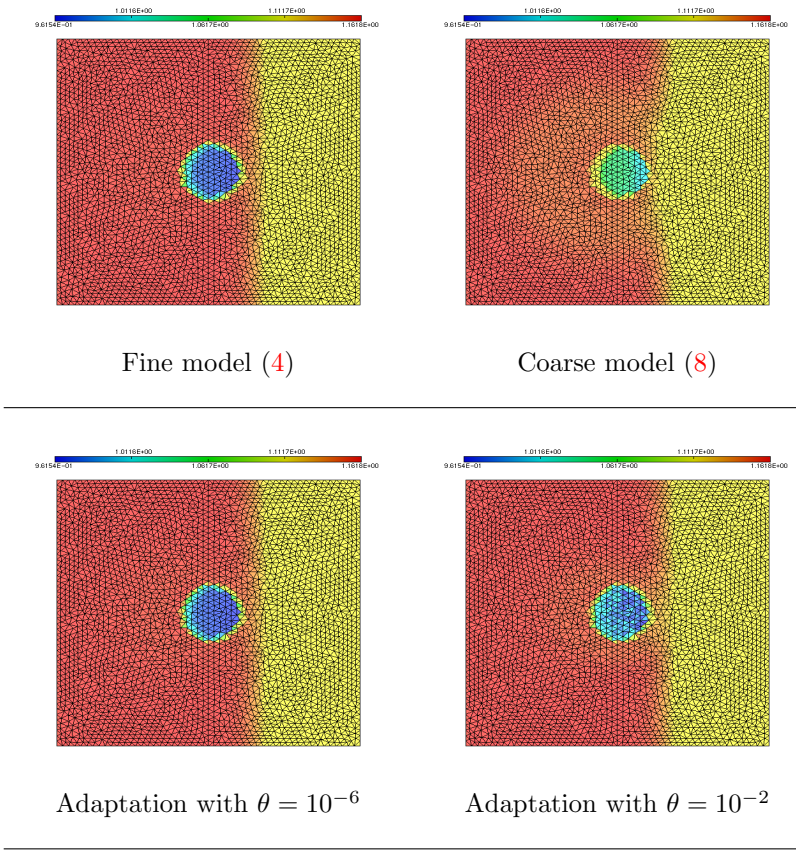

Fine model (4) | Coarse model (8)

Adaptation with $\theta = 10^{-6}$ | Adaptation with $\theta = 10^{-2}$

FIGURE 4. Solution after the first interaction: density ρ

F_2 are Rusanov fluxes, which yields in 2D

$$\begin{aligned}\mathcal{E}_K^{n+1} := \varepsilon\varphi_K^{n+1} = \varepsilon\frac{1}{2|K|}\sum_{L\in\mathcal{N}(K)} |e_{KL}|\,(&\rho_K^n u_K^n \varphi_{eq}(\rho_K^n) + \rho_L^n u_L^n \varphi_{eq}(\rho_L^n)\\ &- a_{KL}(\rho_K^n u_K^n - \rho_L^n u_L^n)\\ &- (\rho\varphi_{eq})'(\rho_K^n)\,(\rho_K^n u_K^n + \rho_L^n u_L^n - a_{KL}(\rho_K^n - \rho_L^n)))\,n_{KL},\end{aligned}$$

where $a_{KL} = \max(|u_K + c_K|, |u_L + c_L|)$ and c_K (resp. c_L) denotes the speed of sound of the fluid in the cell K (resp. the cell L). Note that the indicator $\mathcal{E}_K^{n+1}$ is not a continuous function since φ'_{eq} admits discontinuities at ρ_1^* and ρ_2^*.

Test case. The adaptation algorithm is tested on a 2D (weak) interaction of a bubble with a planar shock wave. The domain is $[-0.5, 0.5]^2$ and the pressure laws are perfect gas equations of state with $\gamma_1 = 1.6$ and $\gamma_2 = 1.5$. Wall boundary conditions are set at the top, right and bottom, while at the left boundary, a Dirichlet condition is prescribed with

$$(\rho, u, v, p, \varphi)(t, x = -0.5, y) = (\rho_2^*, 0.1, 0, 1, 0).$$

The initial data is

$$(\rho, u, v, p, \varphi)(0, x, y) = \begin{cases}(\rho_2^*, 0, 0, 1, 0) & \text{if } x^2 + y^2 < 10^{-2},\\ (\rho_1^*, 0, 0, 1, 1) & \text{else,}\end{cases}$$

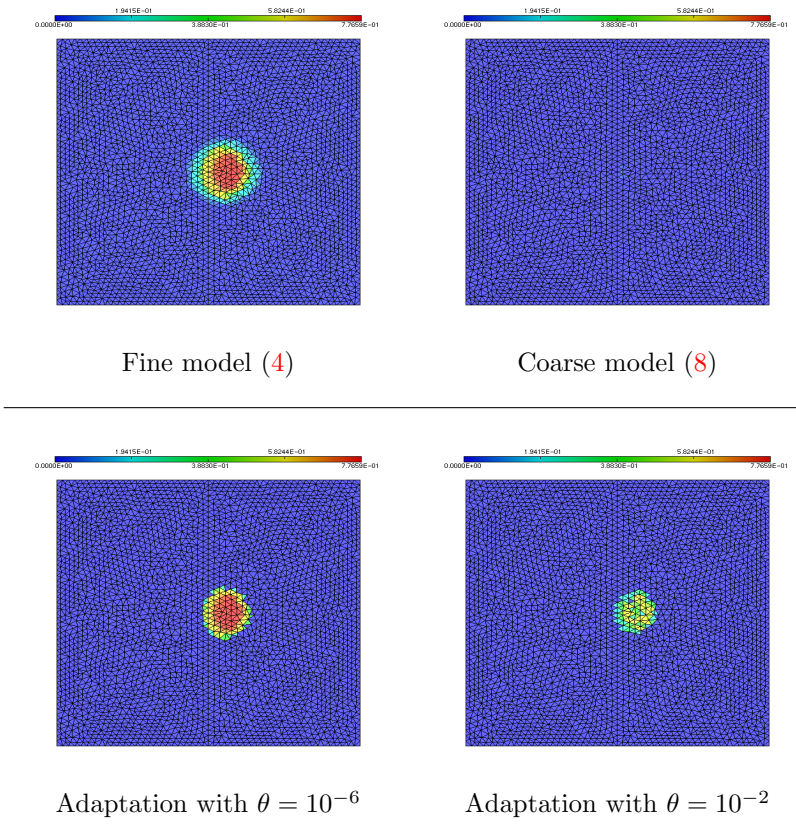

Fine model (4) Coarse model (8)

Adaptation with $\theta = 10^{-6}$ Adaptation with $\theta = 10^{-2}$

FIGURE 5. Solution during the second interaction: mass fraction φ

which corresponds to a bubble of vapor surrounded by the liquid phase. The relaxation time ε is equal to 1. The solution is composed by a shock wave which impacts the bubble, rebounds on the right boundary and impacts once again the bubble. The solution is plotted after the first interaction at $t_1 = 0.6$ and during the second interaction at $t_2 = 1.26$. The mesh is composed of 5906 triangular cells and 3054 vertices. The mass fraction φ is depicted in Figures 3 and 5 while the density ρ is depicted in Figures 4 and 6. In all these figures, we compare the approximate solutions associated with

- the fine model (27),
- the coarse model (28),
- the adaptation algorithm with a threshold $\theta = 10^{-2}$ and
- the adaptation algorithm with a threshold $\theta = 10^{-6}$.

It is clear that the coarse model provides solutions very different from the fine model; in particular, the bubble fully liquefies during the second shock-bubble interaction. The results with $\theta = 10^{-6}$ are more accurate than with $\theta = 10^{-2}$. They are very similar to the results of the fine model, except for the mass fraction at the second time with $\theta = 10^{-6}$ (Fig. 5), where the contours of the bubble are sharper with the adaptation algorithm. Note that, in spite of this difference, the values of ρ and φ inside and outside the bubble are very similar. This behavior can be related with the non-invertibility of the map (7), since transitions between pure phases are present in this test case. This is confirmed by the results of Figure 8, where a saturation

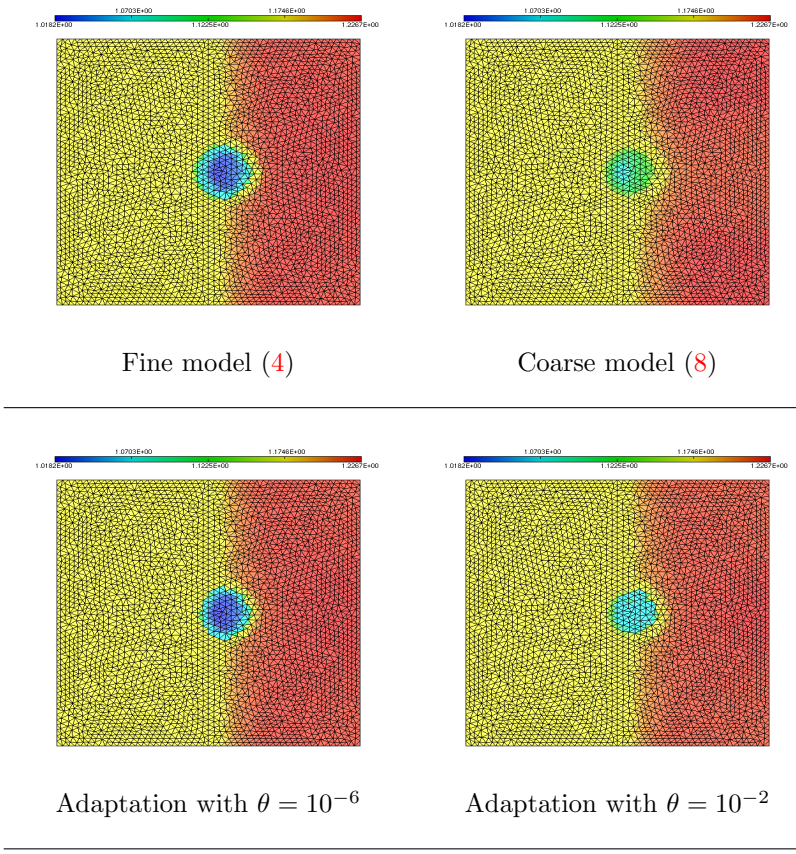

Fine model (4) | Coarse model (8)

Adaptation with $\theta = 10^{-6}$ | Adaptation with $\theta = 10^{-2}$

FIGURE 6. Solution during the second interaction: density ρ

effect occurs when θ tends to 0. Indeed, the error between the fine model and the adaptation algorithm decreases for $\theta \geq 10^{-4}$ but remains constant for smaller values of θ. This appears for both variables φ and ρ and at both times. In Figure 7, the characteristic function of the coarse domain $\mathcal{D}_f$ is plotted for the adaptation algorithm with $\theta = 10^{-2}$ and $\theta = 10^{-6}$, for both times t_1 and t_2. Surprisingly, the results are very close, whatever the threshold θ, except for $\theta = 10^{-6}$ and $t = t_1$, where the fine model is used in the neighborhood of the right boundary.

4.3. **Compressible two-phase flow.** We now consider the computation of a one-dimensional compressible two-fluid flow: each phase is considered as a single phase separated from the other. The two phases have their own thermodynamics and distinct velocities. Thus the balance equations can be given for both phases adding exchange terms between the two phases through the interfaces. This model was first proposed by Baer and Nunziato [9] and then widely studied, see for instance, in a non exhaustive way, Abgrall and Saurel [46], Gallouët *et al* [26], Ambroso *et al* [3], Saleh [45].

Considering our adaptation procedure for such a model is a very challenging benchmark test because this two-fluid flow model does not enter the frame of the previous sections. Indeed we will see that:

- The fine model is non-strictly hyperbolic and non-conservative.
- The source term is non-zero over 3 equations.
- The entropy is not strictly convex.

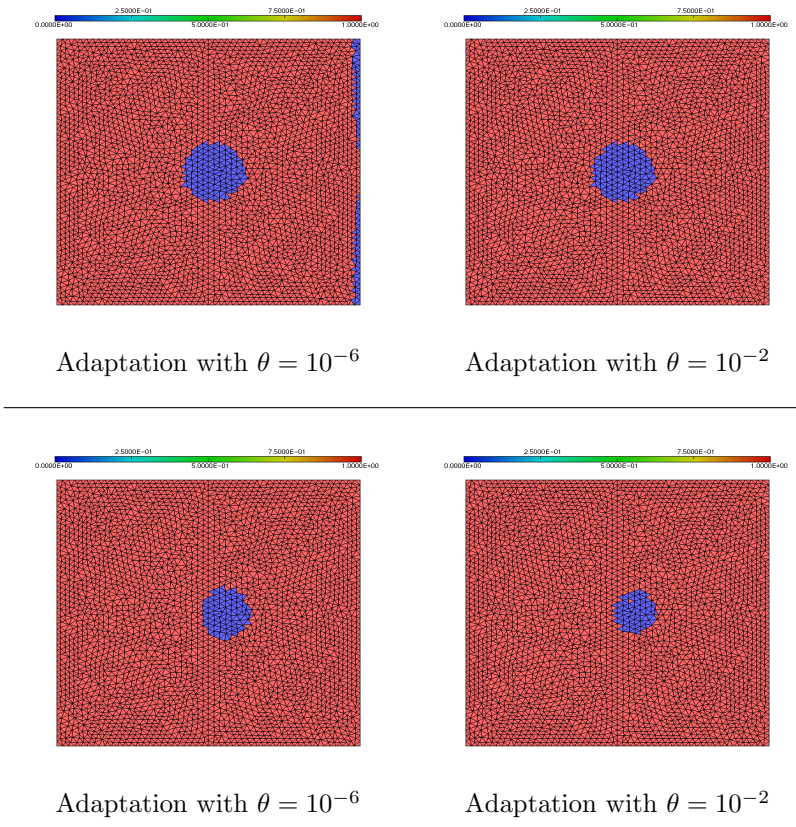

Adaptation with $\theta = 10^{-6}$ Adaptation with $\theta = 10^{-2}$

Adaptation with $\theta = 10^{-6}$ Adaptation with $\theta = 10^{-2}$

FIGURE 7. Partition of the domain between the coarse domain (red) and the fine domain (blue) after the first interaction (up) and during the second interaction (down)

- The Chapman-Enskog expansion is rather complicated and requires adding some assumptions to the system (in particular on the thermodynamics of the two phases).
- The numerical scheme used for the coarse model is not derived from the one of the fine model. Thus the numerical indicator is not deduced from a Chapman-Enskog expansion applied to the numerical scheme.
- The adaptation algorithm has to be modified in order to take into account the non-compatibility of the numerical scheme.

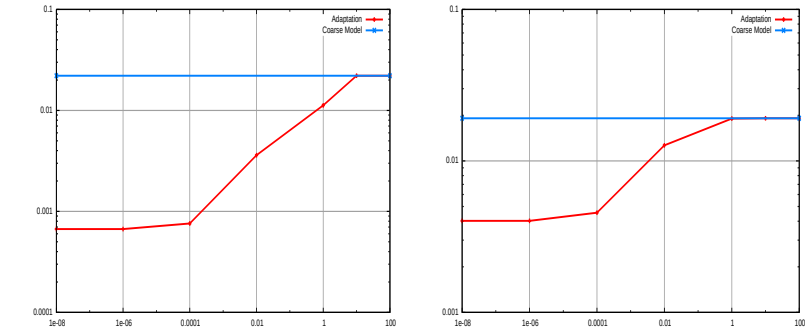

Error for φ Error for ρ

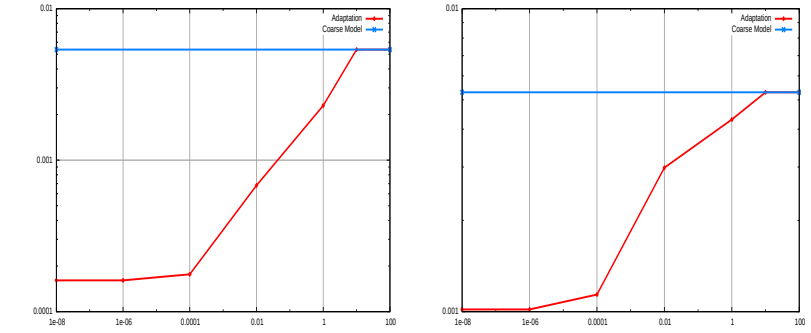

Error for φ Error for ρ

FIGURE 8. Error between model (R) and the model adaptation, w.r.t. θ after the first interaction (up) and during the second interaction (down)

Following [20], the governing set of equations reads in 1D

$$
\begin{cases}
\partial_t \alpha_1 + u_I \partial_x \alpha_1 = \lambda_p (p_1 - p_2), \\
\partial_t (\alpha_1 \rho_1) + \partial_x (\alpha_1 \rho_1 u_1) = 0, \\
\partial_t (\alpha_1 \rho_1 u_1) + \partial_x (\alpha_1 \rho_1 u_1^2 + \alpha_1 p_1) - p_I \partial_x \alpha_1 = -\lambda_u (u_1 - u_2), \\
\partial_t (\alpha_1 \rho_1 E_1) + \partial_x ((\alpha_1 \rho_1 E_1 + \alpha_1 p_1) u_1) - p_I u_I \partial_x \alpha_1 \\
\qquad = -\lambda_T (T_1 - T_2) - u_I \lambda_u (u_1 - u_2) - p_I \lambda_p (p_1 - p_2), \\
\partial_t (\alpha_2 \rho_2) + \partial_x (\alpha_2 \rho_2 u_2) = 0, \\
\partial_t (\alpha_2 \rho_2 u_2) + \partial_x (\alpha_2 \rho_2 u_2^2 + \alpha_2 p_2) - p_I \partial_x \alpha_2 = \lambda_u (u_1 - u_2), \\
\partial_t (\alpha_2 \rho_2 E_2) + \partial_x ((\alpha_2 \rho_2 E_2 + \alpha_2 p_2) u_2) - p_I u_I \partial_x \alpha_2 \\
\qquad = \lambda_T (T_1 - T_2) + u_I \lambda_u (u_1 - u_2) + p_I \lambda_p (p_1 - p_2).
\end{cases} \tag{30}
$$

Here $\rho_k, u_k, p_k, E_k = e_k + \frac{1}{2} u_k^2$ and T_k denote respectively the density, the velocity, the pressure, the total energy (e_k being the internal energy) and the temperature of each phase with $k = 1, 2$. The volume fractions α_k satisfy

$$\alpha_1 + \alpha_2 = 1,$$

so that the two phases are immiscible. Each phase is characterized by its own EoS. We assume for simplicity that both phases are described by perfect gas laws

$$p_k = \pi_k(e_k, \rho_k) = (\gamma_k - 1)\rho_k e_k,$$

where $\gamma_k > 1$ denotes the polytropic exponent. In that case the temperatures satisfy (after normalization $C_v = 1$)

$$T_k = \mathcal{T}_k(e_k, \rho_k) = e_k.$$

The interaction between phases is described with both differential terms and relaxation terms arising in the mass, momentum and total energy equations. The differential terms are non-conservative products that involve an interfacial pressure p_I and an interfacial velocity u_I. These terms depict the coupled evolution of the phases: if $\partial_x \alpha_k = 0$ and the source terms are neglected then the two phases are totally decoupled and each one follows the classical gas dynamics equations. A classical choice for the interfacial pressure and velocity is

$$u_I = u_1, \quad p_I = p_2.$$

Other interfacial closure relations can be chosen, we refer to [26] for detailed explanations.

Let us rewrite the seven-equation model under a form similar to (5-6):

$$\begin{cases} \partial_t U + \partial_x f_1(U,V) = 0, \\ \partial_t V + \partial_x f_2(U,V) + g(U,V)\partial_x \alpha_1 = r(U,V), \end{cases} \tag{31}$$

where

$$\begin{aligned} U &= (\alpha_1\rho_1, \rho, \rho u, \rho E)^T, \\ V &= (\alpha_1, \alpha_1\rho_1 u_1, \alpha_1\rho_1 E_1)^T, \\ r(U,V) &= \begin{pmatrix} \lambda_p(p_1 - p_2) \\ -\lambda_u(u_1 - u_2) \\ -\lambda_T(T_1 - T_2) - u_I\lambda_u(u_1 - u_2) - p_I\lambda_p(p_1 - p_2) \end{pmatrix}, \\ f_1(U,V) &= \begin{pmatrix} \alpha_1\rho_1 u_1 \\ \rho u \\ \rho u^2 + p + \dfrac{\alpha_1\rho_1\alpha_2\rho_2}{\rho}(u_1 - u_2)^2 \\ (\rho E + p)u + \dfrac{\alpha_1\rho_1\alpha_2\rho_2}{\rho}(u_1 - u_2)\left(E_1 + \frac{p_1}{\rho_1} - E_2 - \frac{p_2}{\rho_2}\right) \end{pmatrix}, \\ f_2(U,V) &= \begin{pmatrix} 0 \\ \alpha_1\rho_1 u_1^2 + \alpha_1 p_1 \\ (\alpha_1\rho_1 E_1 + \alpha_1 p_1)u_1 \end{pmatrix}, \\ g(U,V) &= \begin{pmatrix} u_1 \\ -p_2 \\ -p_2 u_1 \end{pmatrix}, \end{aligned}$$

and

$$\begin{aligned} \rho &= \alpha_1\rho_1 + \alpha_2\rho_2, \\ \rho u &= \alpha_1\rho_1 u_1 + \alpha_2\rho_2 u_2, \\ \rho E &= \alpha_1\rho_1 E_1 + \alpha_2\rho_2 E_2, \\ p &= \alpha_1 p_1 + \alpha_2 p_2. \end{aligned} \tag{32}$$

The relaxation terms reflect the fact that the phases are not at kinematic, mechanical and thermodynamical equilibrium. As soon as the time-scales λ_p, λ_T and

λ_u go to $+\infty$, the source term $r(U,V)$ vanishes and the system reaches the equilibrium characterized by

$$\begin{aligned} p_1 &= p_2 = p, \\ u_1 &= u_2 = u, \\ T_1 &= T_2 = T. \end{aligned} \tag{33}$$

Because we consider a perfect gas mixture, the equilibrium of temperatures is equivalent to

$$e_1 = e_2 = e. \tag{34}$$

Thus the map V_{eq} (such that $r(U,V) = 0 \Leftrightarrow V = V_{eq}(U)$) can be written as an explicit function of U:

$$V_{eq}(U) = \begin{pmatrix} \dfrac{(\gamma_1 - 1)\alpha_1\rho_1}{(\gamma_2 - 1)(\rho - \alpha_1\rho_1) + (\gamma_1 - 1)\alpha_1\rho_1} \\ (\alpha_1\rho_1)\dfrac{\rho u}{\rho} \\ (\alpha_1\rho_1)\dfrac{\rho E}{\rho} \end{pmatrix}. \tag{35}$$

This asymptotic limit defines the coarse model

$$\begin{cases} \partial_t(\alpha_1\rho_1) + \partial_x(\alpha_1\rho_1 u) = 0, \\ \partial_t\rho + \partial_x(\rho u) = 0, \\ \partial_t(\rho u) + \partial_x(\rho u^2 + p) = 0, \\ \partial_t(\rho E) + \partial_x((\rho E + p)u) = 0, \end{cases} \tag{36}$$

which corresponds to the classical Euler equations coupled with the evolution equation of the volume fraction α_1.

Combining (33) and (34), we deduce that the equilibrium pressure is also a perfect gas law $p = (\gamma(U) - 1)\rho e$ with

$$\gamma(U) - 1 = (\gamma_2 - 1)\frac{\rho - \alpha_1\rho_1}{\rho} + (\gamma_1 - 1)\frac{\alpha_1\rho_1}{\rho}. \tag{37}$$

We now address the approximation of the fine model (30). The approximation of the seven-equation model has been the subject of many contributions. The numerical scheme we use is adapted from [26, 3]. It consists in treating the convective terms by the Rusanov scheme [44] that handles the non-conservative terms and the relaxation terms by a fractional step approach. Let $Z_K^n = (U_K^n, V_K^n)$ be the one dimensional solution in the cell K at time t^n which we want to update, until time $t^{n,1}$. The non-conservative Rusanov scheme writes

$$\begin{aligned} \Delta x\left((Z)_K^{n,1} - (Z)_K^n\right) + \Delta t\left((F_f)_{K+1/2}^n - (F_f)_{K-1/2}^n\right) \\ - \Delta t(\phi)_K^n\left((\overline{\alpha_1})_{K+1/2}^n - (\overline{\alpha_1})_{K-1/2}^n\right) = 0, \end{aligned} \tag{38}$$

where $F_f = \begin{pmatrix} f_1 \\ f_2 \end{pmatrix}$, f_1 and f_2 being defined in (31), and

$$\begin{aligned} \phi &= (0,0,0,0,u_1,p_2,p_2u_1)^T, \\ 2(F_f)_{K+1/2}^n &= (F_f)_K^n + (F_f)_{K+1}^n - r_{K+1/2}((Z)_{K+1}^n - (Z)_K^n), \\ r_{K+1/2} &= \max(r_K, r_{K+1}), \\ r_K &= \max(|(u_1)_K^n|, |(u_1)_K^n| + (c_1)_K^n, |(u_2)_K^n| + (c_2)_K^n), \\ 2(\overline{\alpha_1})_{K+1/2}^n &= (\alpha_1)_K^n + (\alpha_1)_{K+1}^n. \end{aligned}$$

Here c_k, $k = 1, 2$, denotes the speed of sound of the phase k, which reads

$$c_k = \sqrt{\gamma_k \frac{p_k}{\rho_k}},$$

the phase k following a perfect gas law.

The second step consists in computing the source terms, separating the velocity, the pressure and the temperature relaxations. We recall the main ideas, the whole procedure being widely depicted in [26, 3]. Let $Z^{n,u}$ be the approximation of the solution after the velocity relaxation with $Z^{n,1}$ as initial condition. The velocity relaxation only acts on the velocities u_k and the total energies E_k, $k = 1, 2$:

$$\begin{aligned}
\partial_t(\alpha_1\rho_1) = \partial_t\rho = \partial_t(\rho u) = \partial_t(\rho E) = 0,\\
\partial_t(\alpha_1\rho_1 u_1) = -\lambda_u(u_1 - u_2),\\
\partial_t(\alpha_1\rho_1 E_1) = -\lambda_u(u_1 - u_2),
\end{aligned}$$

which is equivalent, for $k = 1, 2$, to

$$\begin{aligned}
\alpha_k\rho_k\partial_t u_k = (-1)^k\lambda_u(u_1 - u_2),\\
\alpha_k\rho_k\frac{\partial e_k}{\partial p_k}\frac{\partial p_k}{\partial t} = (-1)^k\lambda_u u_1(u_1 - u_2).
\end{aligned}$$

Applying the implicit Euler method to approximate the previous ordinary differential equations leads to the following approximation of the state vector in the cell K between time $t^{n,1}$ and $t^{n,u}$

$$\begin{aligned}
(\alpha_k)_K^{n,u} &= (\alpha_k)_K^{n,1},\\
(\alpha_k\rho_k)_K^{n,u} &= (\alpha_k\rho_k)_K^{n,1},\\
(u_k)_K^{n,u} &= \frac{((\alpha_l\rho_l)_K^{n,1} + \lambda_u\Delta t)(\alpha_k\rho_k u_k)_K^{n,1} + \lambda_u\Delta t(\alpha_l\rho_l u_l)_K^{n,1}}{(\alpha_1\rho_1)_K^{n,1}(\alpha_2\rho_2)_K^{n,1} + \rho_K^{n,1}\lambda_u\Delta t},\\
(p_1)_K^{n,u} &= (p_1)_K^{n,1},\\
(p_2)_K^{n,u} &= (p_2)_K^{n,1} + \frac{\lambda_u\Delta t}{(\gamma_2 - 1)(\alpha_2)_K^{n,1}}((u_1)_K^{n,u} - (u_2)_K^{n,u})^2.
\end{aligned}$$

The pressure relaxation term is now taken into account. From time $t^{n,u}$ to time $t^{n,p}$ the solution is computed by solving the following ODE system

$$\begin{aligned}
\partial_t(\alpha_1\rho_1) = \partial_t(\alpha_1\rho_1 u_1) = 0,\\
\partial_t\rho = \partial_t(\rho u) = \partial_t(\rho E) = 0,\\
\partial_t\alpha_1 = \lambda_p(p_1 - p_2),\\
\alpha_1\rho_1\partial_t E_1 = -p_2\lambda_p(p_1 - p_2).
\end{aligned}$$

Following [26, 3] we use an explicit form of λ_p

$$\lambda_p = \frac{1}{\bar{\lambda}_p}\frac{\alpha_1\alpha_2}{p_1 + p_2},$$

where $\bar{\lambda}_p$ is constant.

Integrating the equations on the total energies gives

$$\begin{aligned}
(p_k - p_l)(t) &= (p_k - p_l)^{n,u}\exp\left(-\lambda_p\int_0^t (A_k - A_l)(\tau)d\tau\right),\\
(p_1p_2)(t) &= (p_1p_2)^{n,u}\exp\left(-\lambda_p\int_0^t \left(\frac{A_1}{p_1}(p_1 - p_2) + \frac{A_2}{p_2}(p_2 - p_1)\right)(\tau)d\tau\right)
\end{aligned}$$

with $A_k = \dfrac{\partial p_k}{\partial \rho_k}\dfrac{\rho_k}{\alpha_k} - \dfrac{\partial p_k}{\partial e_k}\dfrac{p_2}{\alpha_k \rho_k}$. Then multiplying the mass fraction equation by $\frac{1}{\alpha_1 \alpha_2}$ and integrating leads to

$$\left(\frac{\alpha_1}{1-\alpha_1}\right)(t) = \left(\frac{\alpha_1}{1-\alpha_1}\right)^{n,u} \exp\left(\frac{1}{\bar{\lambda}_p}\int_0^t \left(\frac{p_1-p_2}{p_1+p_2}\right)(\tau)d\tau\right).$$

Finally we address the relaxation in temperature and solve the ODE system below between $t^{n,p}$ and t^{n+1}

$$\begin{aligned}\partial_t \alpha_1 = \partial_t(\alpha_1\rho_1) = \partial_t(\alpha_1\rho_1 u_1) = 0,\\ \partial_t \rho = \partial_t(\rho u) = \partial_t(\rho E) = 0,\\ \alpha_1\rho_1\partial_t E_1 = -\lambda_T(T_1 - T_2).\end{aligned}$$

The two phases follow a perfect gas law so that $T_k = e_k$, $k = 1, 2$. Thus the previous equations are equivalent to

$$\alpha_k\rho_k\partial_t e_k = (-1)^k \lambda_T(e_k - e_l), \quad k \neq l.$$

These ordinary differential equations are approximated by

$$(e_k)_K^{n+1} = \frac{((\alpha_l\rho_l)_K^{n,p} + \lambda_T\Delta t)(\alpha_k\rho_k e_k)_K^{n,p} + \lambda_T\Delta t(\alpha_l\rho_l e_l)_K^{n,p}}{(\alpha_1\rho_1)_K^{n,p}(\alpha_2\rho_2)_K^{n,p} + \lambda_T\Delta t\rho_K^{n,p}},$$

for $k \neq l$.

Remark 4.2. *Note that this strategy preserves the positivity of the pressure p_k, the temperature T_k and the maximum principle on the mass fraction $\alpha_k \in [0, 1]$.*

In Section 3 the numerical scheme of the coarse model was deduced from the one of the fine model using the asymptotic preserving property of the fine scheme. In the present case the coarse model has only four equations and is conservative contrary to the fine model. The idea is to use a completely different numerical scheme to approximate the coarse model (36). In the following we consider the classical Rusanov [44] scheme for the approximation of the coarse model. Let U_K^n be the one dimensional solution in the cell K at time t^n to be advanced at time t^{n+1}. The finite volume scheme for the coarse model (35) is

$$\Delta x\left((U)_K^{n+1} - (U)_K^n\right) + \Delta t\left((F_c)_{K+1/2}^n - (F_c)_{K-1/2}^n\right) = 0, \tag{39}$$

together with

$$F_c = \begin{pmatrix}\alpha_1\rho_1 u_1\\ \rho u\\ \rho u^2 + p\\ (\rho E + p)u\end{pmatrix},$$

and

$$\begin{aligned}2(F_c)_{K+1/2}^n &= (F_c)_K^n + (F_c)_{K+1}^n - s_{K+1/2}((U)_{K+1}^n - (U)_K^n),\\ s_{K+1/2} &= \max(s_K, s_{K+1}),\\ s_K &= \max(|(u)_K^n|, |(u)_K^n| + (c)_K^n),\end{aligned} \tag{40}$$

where $c = \sqrt{\gamma p/\rho}$ denotes the speed of sound of the fluid.

The adaptation algorithm relies on the numerical indicator. In section 3, it is deduced via a discrete Chapman-Enskog expansion. Here the complexity of the fine scheme prevents such computations.

To overcome the problem we propose to use a result of [20]. The author performed the Chapman-Enskog expansion on a two-phase model close to (30). Let us recall the result, detailed calculus being given therein.

Proposition 4.1. *Assume that the relaxation process has only one time scale:* $\lambda_u = \lambda_p = \lambda_T = \frac{1}{\varepsilon}$, $\varepsilon > 0$ *fixed. Up to* ε^2 *terms, the smooth solutions of* (30) *satisfy*

$$\begin{aligned} \partial_t(\alpha_1\rho_1) + \partial_x(\alpha_1\rho_1 u) &= \varepsilon\partial_x A, \\ \partial_t\rho + \partial_x(\rho u) &= 0, \\ \partial_t(\rho u) + \partial_x(\rho u^2 + p) &= \varepsilon\partial_x B, \\ \partial_t(\rho E) + \partial_x\left((\rho E + p)u\right) &= \varepsilon\partial_x C, \end{aligned} \tag{41}$$

where, defining $Y_k = \dfrac{\alpha_k\rho_k}{\rho}$,

$$\begin{aligned} A &= \rho(Y_1)^2 Y_2\left(\frac{\rho}{\rho_1} - 1\right)\partial_x p, \\ B &= e(Y_1 - Y_2)^2\partial_x u, \\ C &= \rho e Y_1 Y_2\partial_x p\left(\gamma_1 Y_1\left(\frac{\rho}{\rho_1} - 1\right) + \gamma_2 Y_2\left(\frac{\rho}{\rho_2} - 1\right)\right) + uB. \end{aligned} \tag{42}$$

Note that the non-conservative terms $p_2\partial_x\alpha_k$, $p_2u_1\partial_x\alpha_k$ and the temperature relaxation term are mandatory to compute the Chapman-Enskog expansion. Moreover the first order terms in ε are explicit functions of U.

Then we propose to directly use the L^1-norm of a discrete approximation of the corrector of first order in ε (42) as the numerical indicator (without using the fine numerical scheme as it is done in Section 3). The numerical indicator thus reads

$$\mathcal{E}_K^{n+1} := \varepsilon(|A_K^n| + |B_k^n| + |C_K^n|), \tag{43}$$

together with

$$\begin{aligned} A_K^n &= \rho_K^n((Y_1)_K^n)^2(Y_2)_K^n\left(\frac{(\alpha_1)_K^n}{(Y_1)_K^n} - 1\right)\frac{p_{K+1}^n - p_K^n}{\Delta x}, \\ B_K^n &= e_K^n\frac{u_{K+1}^n - u_K^n}{\Delta x}((Y_1)_K^n - (Y_2)_K^n)^2, \\ C_K^n &= \rho_K^n e_K^n(Y_1)_K^n(Y_2)_K^n\frac{p_{K+1}^n - p_K^n}{\Delta x}\Gamma_K^n + u_K^n B_K^n, \end{aligned}$$

where

$$\Gamma_K^n = \gamma_1(Y_1)_K^n\left(\frac{(\alpha_1)_K^n}{(Y_1)_K^n} - 1\right) + \gamma_2(Y_2)_K^n\left(\frac{(\alpha_2)_K^n}{(Y_2)_K^n} - 1\right).$$

Note that the indicator is written in terms of the vector Z_K^n only, which is fully known in the whole computational domain, so that we can write $\mathcal{E}_K^{n+1} = \mathcal{E}(P_1 Z_K^n)$.

We now address the adaptation algorithm. Because the coarse scheme is not derived from the fine scheme, the adaptation algorithm has to be modified.

We recall that P_1 is the linear operator such that $P_1 Z = U$ and M is the map such that $M(U)$ belongs to the equilibrium manifold $\mathcal{M}$ (see Section 2.1). Let $Z_K^n = (U_K^n, V_K^n)$ be the solution in the cell K known at time t^n which we want to update, until time t^{n+1}. Let $\mathcal{B}_K^n$ be the balance of fluxes in the cell K at time t^n. The 1D adaptation algorithm reads as follows:

A) For all cell K, compute the numerical error $\mathcal{E}_K^{n+1}$ given by (43).
B) For all cell K, if $[E_K^{n+1} > \theta]$ then
   - $K \in \mathcal{D}_f(t^n)$
   Else
   - $K \in \mathcal{D}_c(t^n)$.
C) At this stage, $\overline{\mathcal{D}_f(t^n)} \cup \overline{\mathcal{D}_c(t^n)} = \mathcal{D}\ (= \mathbb{R})$.
   For all interface $K + 1/2$
   - If $[K \in \mathcal{D}_c(t^n)$ and $\forall L \in \mathcal{N}(K), L \in \mathcal{D}_c(t^n)]$

- Compute $(F_c)^n_{K+1/2}$ using the numerical scheme (40).
  Update the balance

$$\mathcal{B}^n_K \leftarrow \mathcal{B}^n_K + (F_c)^n_{K+1/2}$$
$$\mathcal{B}^n_{K+1} \leftarrow \mathcal{B}^n_{K+1} - (F_c)^n_{K+1/2}$$

- Else
  - Compute $(F_f)^n_{K+1/2}$ using the numerical scheme (38).
    Update the balance

$$\mathcal{B}^n_K \leftarrow \mathcal{B}^n_K + (F_f)^n_{K+1/2}$$
$$\mathcal{B}^n_{K+1} \leftarrow \mathcal{B}^n_{K+1} - (F_f)^n_{K+1/2}$$

D) For all cell K

- If $K \in \mathcal{D}_f$
  - $Z^{n+1}_K = Z^n_K - \dfrac{\Delta t}{\Delta x}\mathcal{B}^n_K$
  - Solve the source term
- else
  - $Z^{n+1}_K = M\left(P_1\left(Z^n_K - \dfrac{\Delta t}{\Delta x}\mathcal{B}^n_K\right)\right)$

Test case. We apply this algorithm in the case of the evolution of a two-phase flow in a duct of uniform section and 7m length. The simulation is performed on 1000 cells. The two phases are depicted by a perfect gas law with $\gamma_1 = \gamma_2 = 1.4$. The flow is initially at equilibrium, the initial conditions are $\alpha_1 = 0.9$, $u_1 = u_2 = 5$, $p_1 = p_2 = 10^5$, $\rho_1 = \rho_2 = 1$. A inlet Dirichlet boundary condition is applied on the left side using the initial condition except that $p_1 = 1.005 \times 10^5$ and the relaxation parameters are $\lambda_u = \lambda_p = \lambda_T = \varepsilon^{-1} = 10^4$. A outlet Neumann boundary condition is applied on the right side. These boundary conditions are taken into account using the classical ghost cell method. Finally, the adaptation parameter is $\theta = 10^{-1}$.

This test case allows us to study the asymptotic behavior of the two-phase model. Due to the relaxation terms in the fine model, the relative quantities tend to zero as x increases, leading to a boundary layer on the left. It is worth noting that only the boundary relative pressure is non-zero but the boundary layer also appears for the relative velocity and for the relative temperature. As far as the coarse model is concerned, no relative quantity can be measured and the non equilibrium boundary remains inactive. Figures 9 present the shapes of the relative pressure, velocity and temperature at time $t = 0.2$. One can easily see that the boundary layer is well solved by the fine model and that the relative quantities rapidly tend to 0. In all these cases, the adaptation algorithm provides results which are superposed on the results of the fine model.

Figure 10 presents the evolution of the repartition of the fine and the coarse cells of the adaptation algorithm with respect to time. We can observe that the fine model is mostly applied in the region which corresponds to the boundary layer. A fast right moving set of "fine" cells first appears. It is caused by the formation of the boundary layers, letting small perturbations propagate. After, the domain is split into about two parts: the fine model is used at the left, near the boundary layer, and the coarse model is used at the right. One could expect that, after a long time, the position of the coupling interface should be constant, corresponding to the establishment of the stationary state, but such a behavior has not been observed with the parameters we used.

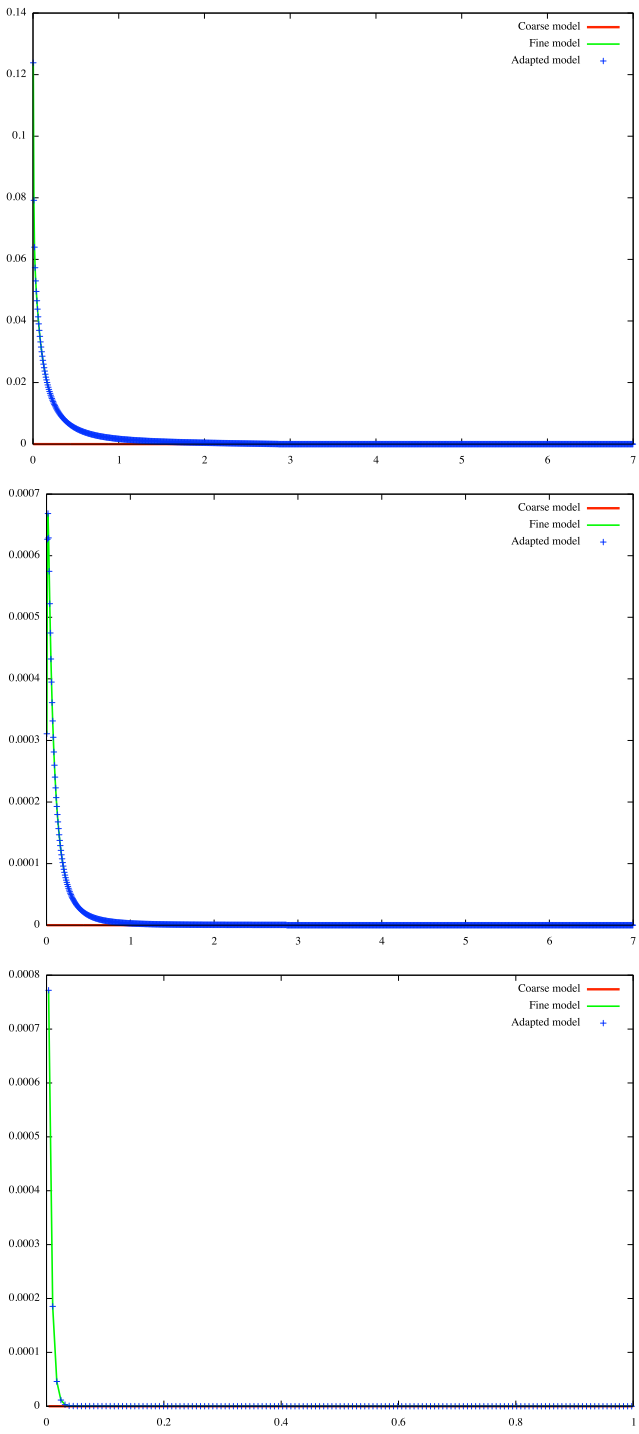

FIGURE 9. Relative velocity (top), relative pressure (middle), relative temperature (zoom, bottom).

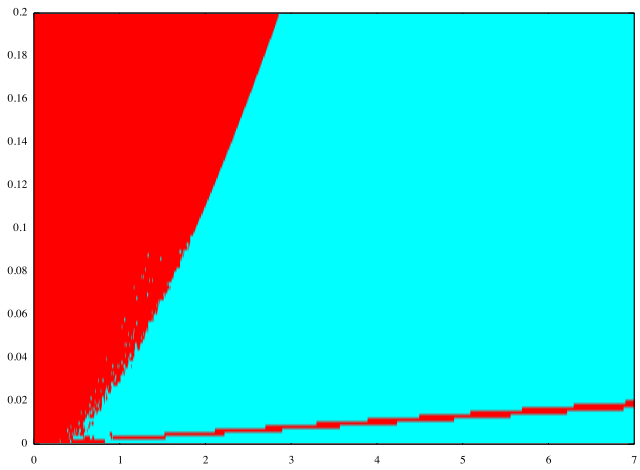

FIGURE 10. Evolution of the indicator (characteristic function of $\mathcal{D}_f(T)$) : repartition of the fine and coarse models in time as a function of x (red: fine model, cyan: coarse model).

5. Conclusion

We propose an original model adaptation algorithm which is rigorously established when applied to hyperbolic systems with relaxation coupled with their asymptotic hyperbolic limit model. Due to the applications under investigation, we are not allowed to modify the numerical schemes for computing both models, which prevents us from using either classical asymptotic preserving schemes on the whole domain or sophisticated micro-macro decompositions. Our method is relies on a numerical Chapman-Enskog expansion, the first order term being used to indicate what model can be selected.

Mainly three test cases are presented in order to assess the relevance of the indicator, in the context of dynamical model adaptation. When the model completely fits the classical assumptions on hyperbolic systems with relaxation, our strategy provides very satisfying results. The use of the coarse model only coincides with the strong variations of the solution. The two other test cases are much more challenging since they do not fully enter in the initial framework. But here again, the indicator allows an accurate dynamical partition of the domain and the adaptation algorithm provides in most cases very close results to the reference solution of the fine model. However, let us recall that, at least in this work, our foremost interest concerns the development of an indicator to determine what model is the more relevant, and not to construct a multiscale method to save CPU time. This is the reason why we do not provide any comparison of efficiency in addition to the studies of accuracy (Figures 2 and 8).

Of course, this indicator is not fully robust: on the one hand, the global error due to the adaptation algorithm cannot be guessed and on the other hand, it is well known that the Chapman-Enskog expansion fails when the solution admits discontinuities. Another issue is that the error due to the interface coupling is not measured. Several works on these topics are under investigation. In particular, a similar adaptive method in the scalar setting is studied, for which rigorous convergence results can be obtained.

Acknowledgments. The authors would like to thank Frédéric Coquel who initially pointed out the issue of model adaptation to them and for fruitful discussions.

This work has been supported by the LRC Manon (Modélisation et approximation numérique orientées pour l'énergie nucléaire – CEA/DM2S-LJLL).

References

[1] A. Abdulle, W. E, B. Engquist, and E. Vanden-Eijnden. The heterogeneous multiscale method. *Acta Numer.*, 21:1–87, 2012.

[2] G. Allaire, G. Faccanoni, and S. Kokh. A strictly hyperbolic equilibrium phase transition model. *C. R. Math. Acad. Sci. Paris*, 344(2):135–140, 2007.

[3] A. Ambroso, Chalons C., and Raviart P.-A. A Godunov-type method for the seven-equation model of compressible two-phase flow. *Comput. & Fluids*, 54:67–91, 2012.

[4] A. Ambroso, C. Chalons, F. Coquel, T. Galié, E. Godlewski, F. Lagoutière, P.-A. Raviart, and N. Seguin. Numerical coupling of two-phase flows. In W. Liu, M. Ng, and Shi Z.-C., editors, *Recent progress in scientific computing (SCPDE, Hong Kong, 2005)*, pages 168–178. Science Press, 2007.

[5] A. Ambroso, C. Chalons, F. Coquel, E. Godlewski, F. Lagoutière, P.-A. Raviart, and N. Seguin. Coupling of multiphase flow models. In *Proceedings of the Eleventh International Meeting on Nuclear Thermal-Hydraulics (NURETH)*, 2005.

[6] A. Ambroso, C. Chalons, F. Coquel, E. Godlewski, F. Lagoutière, P.-A. Raviart, and N. Seguin. Homogeneous models with phase transition: coupling by finite volume methods. In *Finite volumes for complex applications, IV (Marrakech, 2005)*, pages 483–492. Hermes Science, 2005.

[7] A. Ambroso, C. Chalons, F. Coquel, E. Godlewski, F. Lagoutière, P.-A. Raviart, and N. Seguin. The coupling of homogeneous models for two-phase flows. *Int. J. Finite Volumes*, 4(1):1–39, 2007.

[8] A. Ambroso, C. Chalons, F. Coquel, E. Godlewski, F. Lagoutière, P.-A. Raviart, and N. Seguin. Coupling of general Lagrangian systems. *Math. Comp.*, 77(262):909–941, 2008.

[9] M. R. Baer and J. W. Nunziato. A two phase mixture theory for the deflagration to detonation (ddt) transition in reactive granular materials. *Int. J. Multiphase Flow*, 12(6):861–889, 1986.

[10] G. Bal and Y. Maday. Coupling of transport and diffusion models in linear transport theory. *M2AN Math. Model. Numer. Anal.*, 36(1):69–86, 2002.

[11] C. Bernardi, T. C. Rebollo, F. Hecht, and R. Lewandowski. Automatic insertion of a turbulence model in the finite element discretization of the Navier-Stokes equations. *Math. Models Methods Appl. Sci.*, 19(7):1139–1183, 2009.

[12] F. Bouchut. A reduced stability condition for nonlinear relaxation to conservation laws. *J. Hyperbolic Differ. Equ.*, 1(1):149–170, 2004.

[13] B. Boutin. *Étude mathématique et numérique d'équations hyperboliques non-linéaires : couplage de modèles et chocs non classiques*. PhD thesis, Université Pierre et Marie Curie–Paris 6, 2009.

[14] M. Braack and A. Ern. A posteriori control of modeling errors and discretization errors. *Multiscale Model. Simul.*, 1(2):221–238 (electronic), 2003.

[15] F. Caetano. *Sur certains problèmes de linéarisation et de couplage pour les systèmes hyperboliques non linéaires*. PhD thesis, Université Pierre et Marie Curie–Paris 6, France, 2006.

[16] C. Chalons, P.-A. Raviart, and N. Seguin. The interface coupling of the gas dynamics equations. *Quart. Appl. Math.*, 66(4):659–705, 2008.

[17] G. Q. Chen, C. D. Levermore, and T. P. Liu. Hyperbolic conservation laws with stiff relaxation terms and entropy. *Comm. Pure Appl. Math.*, 47(6):787–830, 1994.

[18] F. Coquel, E. Godlewski, and N. Seguin. Relaxation of fluid systems. *Math. Models Methods Appl. Sci.*, 22(8), 2010.

[19] P. Degond, J.-G. Liu, and L. Mieussens. Macroscopic fluid models with localized kinetic upscaling effects. *Multiscale Model. Simul.*, 5(3):940–979 (electronic), 2006.

[20] S. Dellacherie. Relaxation schemes for the multicomponent Euler system. *M2AN Math. Model. Numer. Anal.*, 37(6):909–936, 2003.

[21] G. Dimarco and L. Pareschi. Exponential Runge-Kutta methods for stiff kinetic equations. *SIAM J. Numer. Anal.*, 49(5):2057–2077, 2011.

[22] D. A. Drew and S. Passman. *Theory of Multicomponent Fluids*. Springer, New-York, 1998.

[23] L. Fatone, P. Gervasio, and A. Quarteroni. Multimodels for incompressible flows: iterative solutions for the Navier-Stokes/Oseen coupling. *M2AN Math. Model. Numer. Anal.*, 35(3):549–574, 2001.

[24] F. Filbet and S. Jin. A class of asymptotic-preserving schemes for kinetic equations and related problems with stiff sources. *J. Comput. Phys.*, 229(20):7625–7648, 2010.

[25] T. Galié. *Couplage interfacial de modles en dynamique des fluides. Application aux écoulements diphasiques*. PhD thesis, Université Pierre et Marie Curie–Paris 6, 2009.

[26] T. Gallouët, J.-M. Hérard, and N. Seguin. Numerical modeling of two-phase flows using the two-fluid two-pressure approach. *Math. Models Methods Appl. Sci.*, 14(5):663–700, 2004.
[27] E. Godlewski, K.-C. Le Thanh, and P.-A. Raviart. The numerical interface coupling of nonlinear hyperbolic systems of conservation laws. II. The case of systems. *M2AN Math. Model. Numer. Anal.*, 39(4):649–692, 2005.
[28] E. Godlewski and P.-A. Raviart. The numerical interface coupling of nonlinear hyperbolic systems of conservation laws. I. The scalar case. *Numer. Math.*, 97(1):81–130, 2004.
[29] F. Golse, S. Jin, and C. D. Levermore. A domain decomposition analysis for a two-scale linear transport problem. *M2AN Math. Model. Numer. Anal.*, 37(6):869–892, 2003.
[30] L. Gosse. *Computing Qualitatively Correct Approximations of Balance Laws*. SIMAI Springer Series, 2013.
[31] L. Gosse and G. Toscani. Space localization and well-balanced schemes for discrete kinetic models in diffusive regimes. *SIAM J. Numer. Anal.*, 41(2):641–658 (electronic), 2003.
[32] P. Helluy and H. Mathis. Pressure laws and fast Legendre transform. *Math. Models Methods Appl. Sci.*, 21(4):745–775, 2011.
[33] P. Helluy and N. Seguin. Relaxation models of phase transition flows. *M2AN Math. Model. Numer. Anal.*, 40(2):331–352, 2006.
[34] M. Ishii. *Thermo-fluid dynamic theory of two-phase flow*. Eyrolles, Paris, 1975.
[35] S. Jaouen. *Étude mathématique et numérique de stabilité pour des modèles hydrodynamiques avec transition de phase*. PhD thesis, Université Pierre et Marie Curie-Paris 6, France, 2001.
[36] S. Jin. Efficient asymptotic-preserving (AP) schemes for some multiscale kinetic equations. *SIAM J. Sci. Comput.*, 21(2):441–454 (electronic), 1999.
[37] S. Jin. Asymptotic preserving (AP) schemes for multiscale kinetic and hyperbolic equations: a review. *Riv. Math. Univ. Parma (N.S.)*, 3(2):177–216, 2012.
[38] S. Jin, J.-G. Liu, and L. Wang. A domain decomposition method for semilinear hyperbolic systems with two-scale relaxations. *Math. Comp.*, posted on October 9, 2012.
[39] F. Kissling and C. Rohde. The computation of nonclassical shock waves with a heterogeneous multiscale method. *Netw. Heterog. Media*, 5(3):661–674, 2010.
[40] A. Klar. An asymptotic preserving numerical scheme for kinetic equations in the low Mach number limit. *SIAM J. Numer. Anal.*, 36(5):1507–1527 (electronic), 1999.
[41] M. Lemou and L. Mieussens. A new asymptotic preserving scheme based on micro-macro formulation for linear kinetic equations in the diffusion limit. *SIAM J. Sci. Comput.*, 31(1):334–368, 2008.
[42] T. P. Liu. Hyperbolic conservation laws with relaxation. *Comm. Math. Phys.*, 108(1):153–175, 1987.
[43] H. Mathis and N. Seguin. Model adaptation for hyperbolic systems with relaxation. In *Finite volumes for complex applications, VI (Prague, 2011)*, pages 673–681. Springer, 2011.
[44] V. V. Rusanov. The calculation of the interaction of non-stationary shock waves with barriers. *Ž. Vyčisl. Mat. i Mat. Fiz.*, 1:267–279, 1961.
[45] K. Saleh. *Analyse et simulation numrique par relaxation d'écoulements diphasiques compressibles. Contribution au traitement des phases évanescentes*. PhD thesis, Université Pierre et Marie Curie–Paris 6, 2012.
[46] R. Saurel and R. Abgrall. A multiphase Godunov method for compressible multifluid and multiphase. *Journal of Computational Physics*, 150(2):425–467, 1999.
[47] D. Serre. Multidimensional shock interaction for a Chaplygin gas. *Arch. Ration. Mech. Anal.*, 191:539–577, 2009.
[48] I. Suliciu. On the thermodynamics of rate-type fluids and phase transitions. *Internat. J. Engrg. Sci.*, 36:921–947, 1998.
[49] A. E. Tzavaras. Relative entropy in hyperbolic relaxation. *Commun. Math. Sci.*, 3(2):119–132, 2005.
[50] W.-A. Yong. Singular perturbations of first-order hyperbolic systems with stiff source terms. *J. Differential Equations*, 155(1):89–132, 1999.

Hélène Mathis
Université de Nantes, Laboratoire de Mathématiques Jean Leray, 2, Rue de la Houssinière, 44322 Nantes Cedex 03, France
helene.mathis@univ-nantes.fr

Clément Cancès, Edwige Godlewski
UPMC Univ Paris 06, UMR 7598, Laboratoire Jacques-Louis Lions, F-75005, Paris, France
CNRS, UMR 7598, Laboratoire Jacques-Louis Lions, F-75005, Paris, France
cances@ann.jussieu.fr, godlewski@ann.jussieu.fr

Nicolas Seguin (corresponding author)
INRIA Rocquencourt, BP 105, F-78153, Le Chesnay Cedex, France
UPMC Univ Paris 06, UMR 7598, Laboratoire Jacques-Louis Lions, F-75005, Paris, France
CNRS, UMR 7598, Laboratoire Jacques-Louis Lions, F-75005, Paris, France
nicolas.seguin@upmc.fr
Phone: +33 1 44 27 37 72
Fax: +33 1 44 27 72 00